ELSEVIER

Remote Sensing of Environment 78 (2001) 131–149

Remote Sensing of Environment

www.elsevier.com/locate/rse

Coupling a grassland ecosystem model with Landsat imagery for a 10-year simulation of carbon and water budgets

Yann Nouvellon[a,*], M. Susan Moran[a], Danny Lo Seen[b], Ross Bryant[a], Serge Rambal[c], Wanmei Ni[a], Agnès Bégué[b], A. Chehbouni[d], William E. Emmerich[a], Phil Heilman[a], Jiaguo Qi[e]

[a]*USDA-ARS-SWRC, Tucson, AZ, USA*
[b]*CIRAD-AMIS/Maison de la Télédétection, Montpellier, France*
[c]*CEFE-CNRS, DREAM Unit, Montpellier, France*
[d]*CESBIO-(CNES-CNRS-UPS-IRD), Toulouse, France*
[e]*Michigan State University, East Lansing, MI, USA*

Received 20 January 2000; received in revised form 12 February 2001; accepted 30 April 2001

Abstract

In this study, high-spatial, low-temporal scale visible remote sensing data were used to calibrate an ecosystem model (EM) for semiarid perennial grasslands. The model was driven by daily meteorological data and simulated plant growth and water budget on the same time step. The model was coupled with a canopy reflectance model to yield the time course of shortwave radiometric profiles. Landsat Thematic Mapper (TM) and Enhanced TM Plus (ETM+) images from 10 consecutive years were used to refine the model on a spatially distributed basis. A calibration procedure, which minimized the difference between the normalized difference vegetation index (NDVI) simulated from the coupled model and measured by the TM and ETM+ sensors, yielded the spatial distribution of an unknown parameter and initial condition. Accuracy of model products, such as daily aboveground biomass, leaf area index (LAI) and soil water content, was assessed by comparing them with field measurements. The promising results suggest that this approach could provide spatially distributed information about both vegetation and soil conditions for day-to-day grassland management.

1. Introduction

Ecosystem models (EM) have the ability to represent important processes and variables such as plant growth, crop yield, and soil water fluxes. Although their performance and accuracy have continuously improved over the past few years, there are still few operational applications in agriculture, forestry, and rangeland management. In most cases, operational applications have been hampered by the inability to provide a spatial distribution of the complete set of required model parameters and initial conditions (e.g., Boote, Jones, & Pickering, 1996; Franks & Beven, 1999; Inoue, Moran, & Horie, 1997).

At the same time, satellite and airborne sensors offer an increasing amount of information about the space–time behavior of land surfaces, with measurements over most of the electromagnetic spectrum, at different view angles, and under a large range of spatial and temporal resolutions. This explains the growing interest in developing methods to use remotely sensed information in EM (e.g., Delécolle, Maas, Gueril, & Baret, 1992; Fisher, Kergoat, & Dedieu, 1997; Maas, 1988a,b; Moran, Maas, & Pinter, 1995; Rambal, Lacaze, Mazurek, & Debussche, 1985; Running et al., 1989, 1999). One of the most effective methods is to derive fields of calibration parameters by minimizing the difference between the space–time behavior of the surface measured by the sensor and simulated by the EM combined with a radiative transfer model (RTM) (e.g., Bouman, 1992; Moulin, Bondeau, & Delécolle, 1998).

The feasibility of using remotely sensed data for model calibration has been demonstrated with reflectance (e.g., Clevers, Büker, Van Leeuwen, & Bouman, 1994; Nouvellon, 1999), infrared brightness temperature (Olioso, Taconet, & Ben Mehrez, 1996; Taconet, Olioso, Ben Mehrez, & Brisson, 1995), active or passive microwave (Burke, Gurney, Simmonds, & Jackson, 1997; Camillo, O'Neil, & Gurney, 1986), or a combination (e.g., radar and visible

* Corresponding author. s/c Anne Catillon, Programme Arbres et Plantations, CIRAD-FORET, TA 10/C, Baillarguet, 34398 Montpellier, Cedex 5, France. Tel.: +33-4-67-59-37-51; fax: +33-4-67-59-37-33.
E-mail address: cir12@calva.com (Y. Nouvellon).

0034-4257/01/$ – see front matter
PII: S0034-4257(01)00255-3

(Bouman, 1992); visible and thermal (Cayrol, Moulin, Kergoat, Dedieu, & Chehbouni, 1999)). In most cases, feasibility studies have been carried-out using mostly ground-based sensor measurements, and in some cases point-based satellite measurements. Feasibility studies and operational applications using satellite-based images are much fewer, due to three main reasons:

- mismatch between the scales of ground sampling, management needs, and satellite images;
- unavailable spatially distributed input parameters such as meteorological inputs and data for atmospheric characterization;
- current satellite-based sensors do not provide data with both a high spatial resolution and a high temporal resolution. Sensors with high temporal resolution (e.g., NOAA-AVHRR, VEGETATION) have coarse spatial resolution, resulting in cumbersome and still unsolved problems of mixed pixels.

Plant and soil processes operate at short time scale, implying that remotely sensed data should be acquired frequently enough to capture their dynamics. At the same time, for most applications (e.g., rangeland management), processes and state variables have to be described at fine spatial resolution. For instance, range managers are interested in the spatial and temporal variations of plant biomass and soil moisture over their ranch (Tueller, 1989). This spatially distributed information about soil and vegetation condition is useful for predicting and managing livestock distribution and erosion risk (Hanson, Skiles, & Parton, 1988).

For semiarid perennial grasslands such as shortgrass ecosystems that cover large areas in the southwest United States, EM have been developed that allow multiyear simulations of plant growth patterns by accounting for carbohydrate storage in the root system and further translocation to aboveground regrowth (e.g., Bachelet, Hunt, & Detling, 1989; Detling, Parton, & Hunt, 1979; Hanson et al., 1988; Nouvellon, Rambal, et al., 2000). With multiyear simulations, high-spatial, low-temporal scale remotely sensed data collected over several consecutive years may provide sufficient information for calibrating an EM with a spatial resolution that matches range managers' requirements.

The objective of this paper was to show the feasibility of this approach. An EM consisting of a plant growth and a soil water budget submodel and combined with a RTM was applied over a semiarid grassland watershed in southeastern Arizona using soil maps and measured daily input meteorological data. Simulations were performed over a 10-year period. Landsat Thematic Mapper (TM) and Enhanced TM Plus (ETM+) images obtained during these 10 consecutive years were used to refine the model to work on a spatially distributed basis through a calibration procedure, which minimized the difference between the surface reflectances simulated by the model and those measured by the TM and ETM+ sensors.

2. Study area and data description

The study was conducted on the Walnut Gulch Experimental Watershed (WGEW; 31°43′N 110°W) within the San Pedro Basin, southeastern Arizona. This relatively small watershed (150 km^2) has been intensively monitored and studied by the USDA-ARS Southwest Watershed Research Center since 1954 (Renard et al., 1993). Topography is typified as gently rolling hills and elevation ranges from 1225 to 1950 m above sea level. The annual precipitation ranges from 250 to 500 mm with approximately two-thirds falling during the "monsoon season" from July to September (Osborn, Lane, & Hundley, 1972). Summer precipitation is characterized by convective thunderstorms of limited extent resulting from moist unstable air masses coming from the Gulf of Mexico, whereas winter precipitation results from frontal storms characterized by long duration, low intensity, and large area coverage (Sellers & Hill, 1974). Over the year, daily global radiation and photosynthetically active radiation (PAR) are 19.1 and 9.0 MJ, respectively. Maximum global radiation occurs in June (26.8 MJ day^{-1}) and the minimum in December (10.0 MJ day^{-1}). The mean annual temperature is about 16.7°C and the mean monthly temperature ranges from 8°C to 27°C. Relative air humidity is low throughout the year (average value = 39.5%). The mean annual wind is about 3.6 m s^{-1}.

The lower two-thirds of the watershed is mostly dominated by shrubby vegetation representative of the Chihuahuan desert. The upper third of the watershed is mostly dominated by C_4 perennial grasses whose dominant species are black grama (*Bouteloua eriopoda* (Torr.) Torr.), curly mesquite (*Hilaria belangeri* (Steud.) Nash), hairy grama (*Bouteloua hirsuta* (Lag.)), blue grama (*Bouteloua gracilis* (H.B.K.) Lag. ex Steud.), sideoats grama (*Bouteloua curtipendula* (Michx.) A. Gray), and three-awn (*Aristida hamulosa* (Henr.)) (Goff, 1985; Weltz, Ritchie, & Fox, 1994). A vegetation map (20-m resolution) was available for selecting the areas covered by grasslands, as well as a soil map, that describes the repartition of 24 soil classes with 20-m spatial resolution, with percent sand, clay and loam given at different layers (Breckenfeld, Svetlik, & McGuire, 1995).

Since 1990, the Kendall site, central to the grassland area, has been instrumented by the ARS to provide continuous measurement of local meteorological conditions. Rainfall was monitored using automated weighing rain gauges (Renard et al., 1993). Other ancillary meteorological data included wind speed, measured at 2 m aboveground level (AGL) using a R.M. Young photochopper cup anenometer, global incoming solar radiation, measured at 3.5 m AGL using a LiCor silicon pyranometer model LI-200SZ, and relative air humidity and air temperature, measured at 2 m AGL using a Campbell Scientific (CSI) temperature and relative humidity sensor model 207 contained in a Gill radiation shield (Kustas et al., 1994; Kustas & Goodrich, 1994). Net radiation was also measured, at 3.3 m AGL with

a REBS Q*6 net radiometer (Kustas et al., 1994; Stannard et al., 1994), as well as soil water content from time domain reflectometry (TDR) probes spaced every 10 cm down to a depth of 60 cm (Amer, Keefer, Weltz, Goodrich, & Bach, 1994). Aboveground biomass and LAI were estimated at the Kendall site at 2-week to 1-month intervals during the growing seasons of 1990, 1991, 1992, and 1999, and at approximately 1.5-month intervals between summer growth periods in 1990, 1991, and 1992 (Tiscareno-Lopez, 1994). In 1999, aboveground biomass was also estimated at several other sites, scattered over the WGEW, and georeferenced with a global positioning system (GPS). Each estimation of live and dead standing biomass resulted from clipping plants within eight 0.5×1.0 m quadrats (1.0×1.0 m quadrats in 1999), and weighing them after a 24-h drying period at 70°C.

Landsat TM and ETM+ images were acquired during summer growing seasons (approximately 3 months) between 1990 and 1999. Due to infrequent TM and ETM+ overpasses and frequent cloudy conditions, there were between two and four clear images available for each growing season (29 images for the 10-year period). Additional images were obtained during the dry season in May and June for soil optical properties assessment. At the Kendall site, prior to the growing season in June 1990, ground-based soil bidirectional reflectances were obtained with an Exotech radiometer (with spectral filters covering 0.45–0.52 μm (blue), 0.53–0.61 μm (green), 0.62–0.69 μm (red), and 0.78–0.90 μm (NIR), similar to visible bands of TM sensor) using a BRDF apparatus designed by the USDA Water Conservation Lab in Phoenix, Arizona (Jackson et al., 1990). During 1990 and 1992 growing seasons, coincident to TM overpasses, nadir reflectance measurements along transects were also made at the Kendall site, from a height of approximately two meters, using a yoke-based Exotech (Moran et al., 1994).

3. Ecosystem model

The EM used in this study (Nouvellon, 1999; Nouvellon, Lo Seen, et al., 2000; Nouvellon, Rambal, et al., 2000) is schematically described in Fig. 1. The model is driven by standard daily meteorological data and simulates on a daily basis the biomass dynamics of green shoots, dead shoots and living roots. Plant transpiration, evaporation from bare

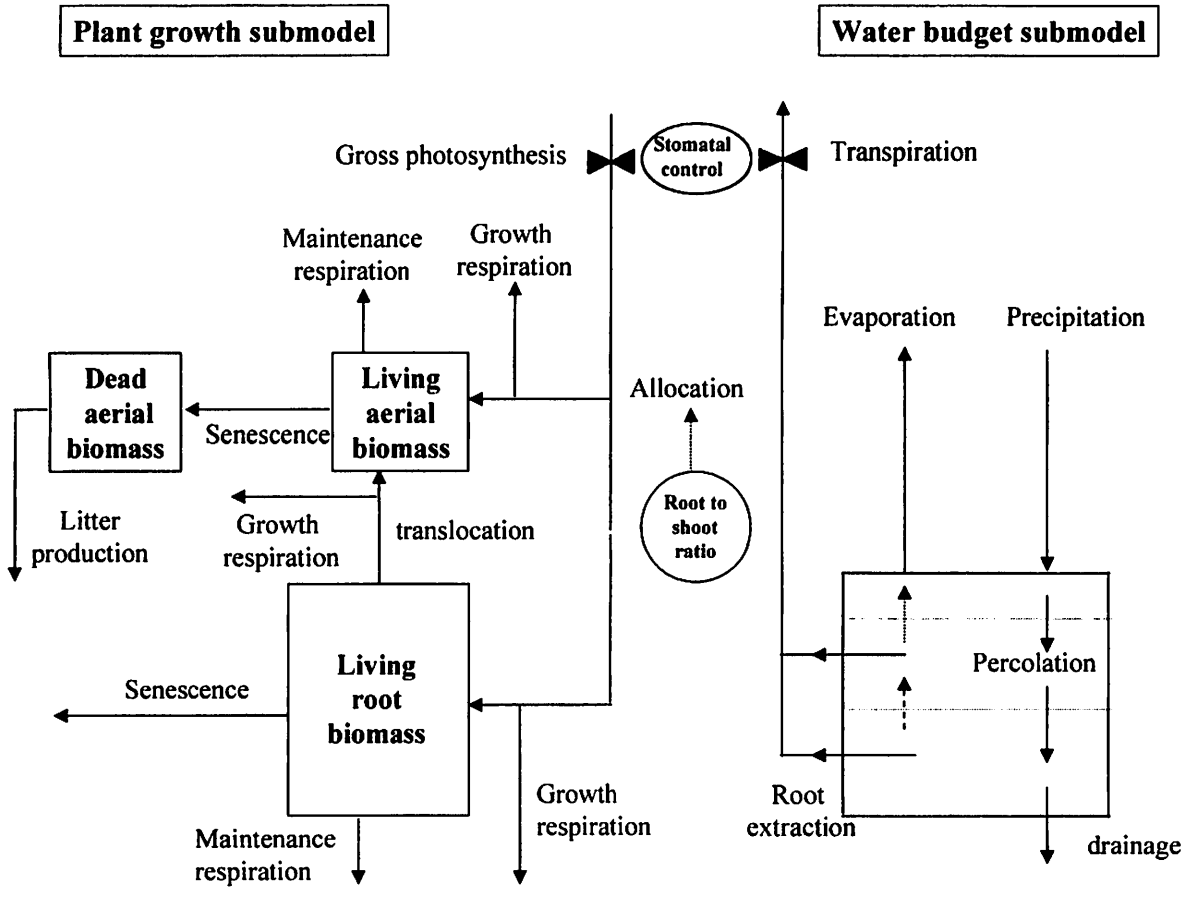

Fig. 1. Schematic representation of the plant growth and water budget models.

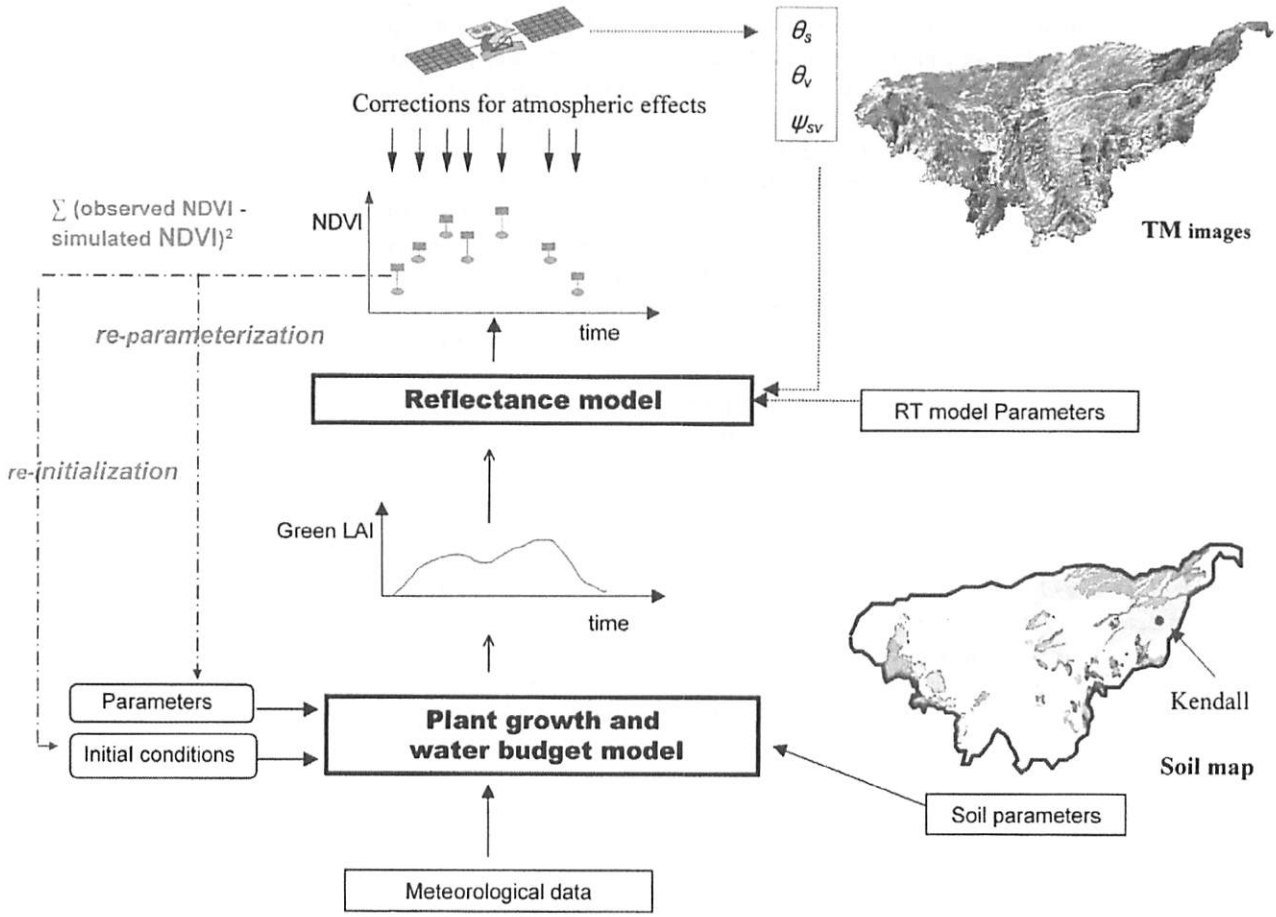

Fig. 2. Synoptic view of the approach used to refine the plant growth/soil water budget model to work on a spatially distributed basis using time series of Landsat TM and ETM+ images.

soil, and soil water fluxes are also simulated in a water budget submodel. The plant growth and water budget submodels were coupled with a RTM. The main features of the three submodels are presented here.

3.1. Plant growth

The main processes simulated in the plant growth submodel are photosynthesis, photosynthate partitioning between aerial and belowground compartments, translocation of carbohydrates from roots to shoots during the regrowth period, autotrophic respiration and senescence. The time course of biomass in the three carbon compartments is described by a set of three differential equations with respect to time t (Eq. (1)):

$$\begin{cases} \frac{dB_{ag}}{dt} = a_a P_g + T_{ra} - R_{at} - S_a \\ \frac{dB_r}{dt} = a_r P_g - T_{ra} - R_{rt} - S_r \\ \frac{dB_{ad}}{dt} = S_a - L \end{cases}, \quad (1)$$

where B_{ag}, B_r, and B_{ad} are living aboveground biomass, living root biomass, and standing dead biomass (expressed in g DM m^{-2}), respectively; P_g is the daily gross photosynthesis; a_a and a_r are the photosynthate allocation partition coefficients to shoot and root compartments ($a_a + a_r = 1$); T_{ra} represents the translocation of carbohydrates from the roots to the living aboveground compartment at the regrowth period; R_{at} and R_{rt} are total daily amounts of respiration (the sum of growth and maintenance respirations) from aboveground and root compartments; S_a and S_r represent the losses of biomass of the living shoots and roots due to senescence, and L represents the litter fall. A detailed description of the equations (and coefficients) used to compute a_a, a_r, T_{ra}, P_g, R_{at}, R_{rt}, S_a, S_r, and L can be found in Nouvellon (1999) and Nouvellon, Rambal, et al. (2000). However, to introduce a parameter that will be important further in this study, it is necessary here to describe how the gross daily canopy photosynthesis, P_g, is computed. It is expressed as (Eq. (2)):

$$P_g = \varepsilon_g(\mathrm{PAR} f_{\mathrm{APAR}}), \quad (2)$$

where PAR is the daily incoming PAR (MJ m^{-2}), f_{APAR} represents the fraction of PAR that is absorbed by green leaves (Goward & Huemmrich, 1992), and ε_g is the canopy energy conversion efficiency (or g assimilated dry matter (DM) per unit of absorbed PAR (APAR)). The complete set of equations used to compute f_{APAR} as a function of green leaf area index (GLAI), canopy structure, soil albedo, and leaf optical properties can be found in Nouvellon, Bégué, et al. (2000). For gross photosynthesis, the canopy energy conversion efficiency, ε_g, is expressed as:

$$\varepsilon_g = \varepsilon_{gmax} f_1(T) f_2(\Psi_1) f_3(\text{age}), \quad (3)$$

where $f_1(T)$, $f_2(\Psi_1)$, and f_3(age) represent the effects of suboptimal temperatures, water stress, and leaf aging (Nouvellon, 1999; Nouvellon, Lo Seen, et al., 2000; Nouvellon, Rambal, et al., 2000); $\varepsilon_{g\ max}$ is the potential energy conversion efficiency, for young mature tissues, with optimal temperatures, and in the absence of water stress. The water stress function, $f_2(\Psi_1)$, is computed from mesophyll resistance to CO_2 diffusion, the minimum and actual canopy stomatal resistance to water vapor ($r_{sc\ min}$ and r_{sc}), the canopy boundary layer aerodynamic resistance of water vapor (r_a), and the ratio of diffusivities of CO_2 and water vapor in the air (Mougin, Lo Seen, Rambal, Gaston, & Hiernaux, 1995; Nouvellon, Rambal, et al., 2000; Rambal & Cornet, 1982). These latter resistances (r_{sc} and r_a) are computed in the water budget submodel.

From model simulations, gross, net, and aboveground net primary productivities (GPP, NPP, and ANPP, respectively) can be computed over different time periods. NPP is obtained from the GPP (the time integral of gross photosynthesis) by subtracting maintenance and growth respiration. ANPP is computed as the amount of carbohydrates allocated to aboveground parts of the vegetation (both through gross photosynthesis and translocation from roots to shoots) minus respiration from aboveground parts (Nouvellon, Lo Seen, et al., 2000).

3.2. Water budget

The water balance submodel uses a simplified two layer canopy evaportranspiration model where the soil profile is divided into three layers: a thin superficial layer (0–2 cm) which is supposed to participate only in the soil evaporation

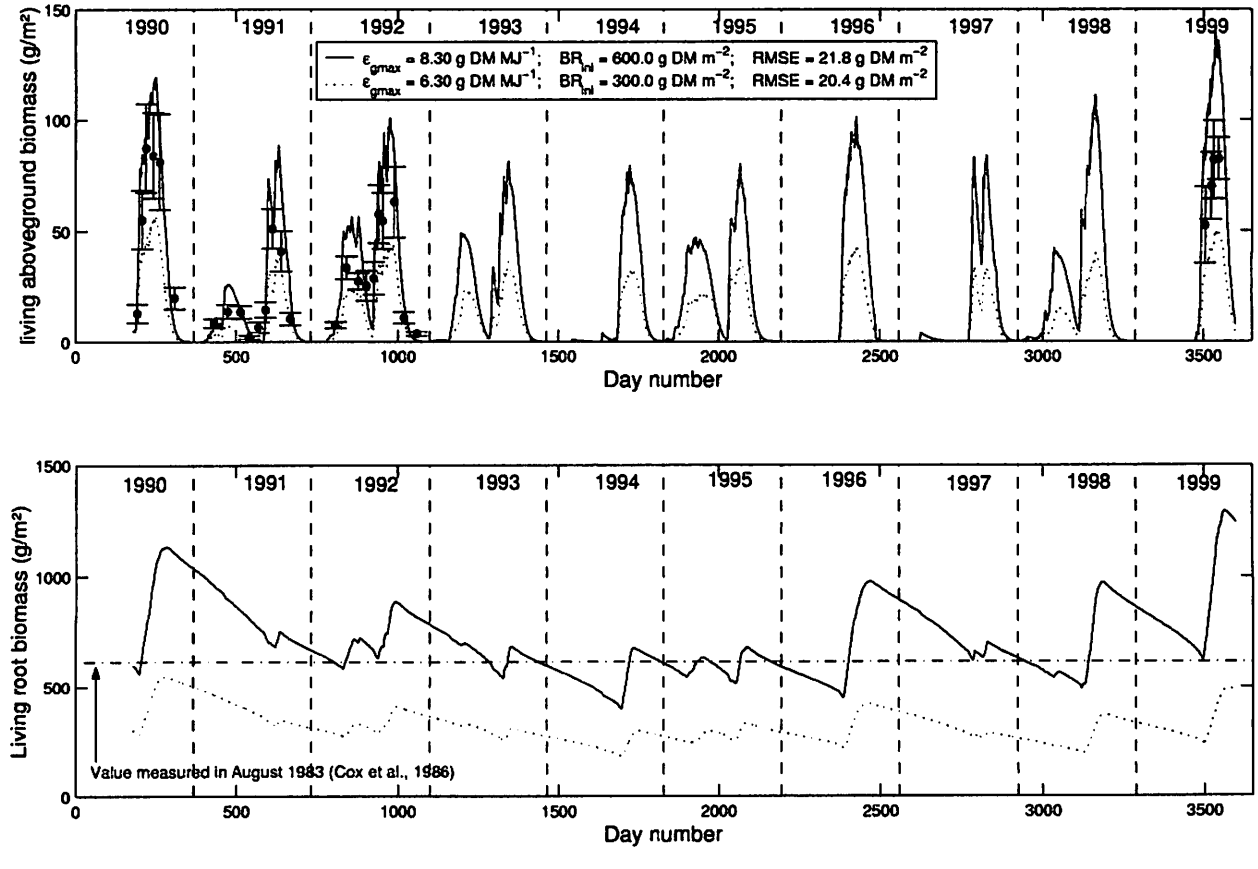

Fig. 3. Simulation results obtained using two a-priori sets of reasonable values of ε_{gmax} and BR_{ini} (continuous lines). In the top graph, solid circles with error bars show aboveground biomass measurements. In the bottom graph, the horizontal broken line show the value of root biomass measured by Cox et al. (1986) in August 1983. The RMSE associated to each set of parameters are indicated on the graphs.

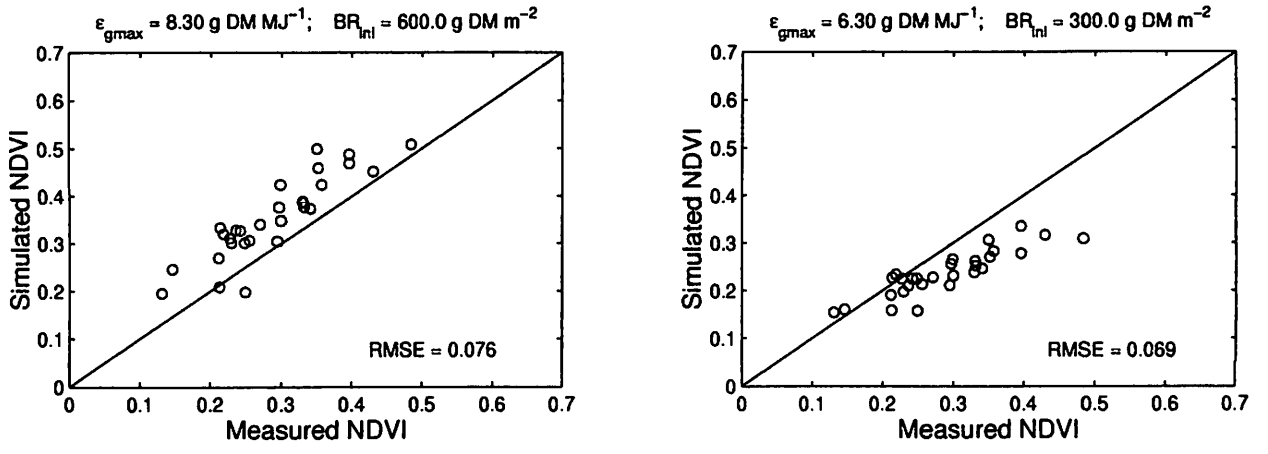

Fig. 4. Comparison of the NDVI simulated with two a-priori sets of reasonable values of ε_{gmax} and BR_{ini} and the NDVI measured by TM and ETM+ sensor.

process E_S, and two deeper layers (2–15 and 15–60 cm) corresponding to the root zone, which participate both in the evaporation and transpiration processes. Each soil layer is characterized by its water content and water potential. These two variables are related by a widely used power-function model for the retention curve (Brooks & Corey, 1964; Campbell, 1974; Saxton, Rawls, Romberger, & Papendick, 1986) whose coefficients are computed as a function of soil particle size distribution in each soil layer using the broad-based regression equations proposed by Saxton et al. (1986). Changes in soil water content in each layer are simulated by a multilayered bucket model with a daily time step (Nouvellon, 1999; Nouvellon, Rambal, et al., 2000; Rambal & Cornet, 1982).

The total evaporation from the sparse grass canopy is calculated as the sum of bare soil evaporation E_S and of canopy evapotranspiration E_C. E_C and E_S are calculated empirically from the evapotranspiration of a continuous canopy, and evaporation of a bare soil, following Penman–Monteith equations (Monteith, 1965) and taking into account the proportion of the surface which is covered by green vegetation and bare soil. The mean leaf water potential needed to calculate the canopy stomatal resistance r_{sc} (used in the Penman–Monteith equations) is obtained iteratively assuming that the total water uptake (the sum of water uptakes in each soil layer, computed from leaf and soil water potentials using Ohm's law analogies (e.g., Lhomme, 1998)) equals transpiration (Nouvellon, 1999; Nouvellon, Rambal, et al., 2000; Rambal & Cornet, 1982). Water extraction in each layer depends on root density, computed from total living root biomass and the root distribution functions from Jackson et al. (1996), whose coefficient has been fitted to measurements obtained at the Kendall site (Cox, Frasier, & Renard, 1986) and nearby sites (Nouvellon, 1999).

The plant growth and water budget submodels have been validated with soil water, biomass and LAI measurements acquired on several short-grass ecosystem sites in southeast Arizona and northeast Sonora (Nouvellon, 1999; Nouvellon, Rambal, et al., 2000).

3.3. Canopy reflectance

In the case of sparse shortgrass canopies, accuracy of RTM is improved if the model accounts for canopy clumping (e.g., Bégué, Luquet, Dauzat, & Nouvellon, 2001; Luquet, Bégué, Dauzat, Nouvellon & Rey, 2001; Nouvellon, Bégué, et al., 2000). Model accuracy also depends on its ability to account for soil nonlambertian properties due to large gap fractions in the canopy.

Based on these considerations, the Markov Chain of Canopy Reflectance (MCCR) model (Kuusk, 1995a) was selected. The MCCR model accounts for the nonrandom pattern of leaf distribution through the incorporation of a Markov model for gap fractions computation (Eq. (4)):

$$T(\theta) = \exp[-\lambda(\theta)k(\theta)\mathrm{LAI}], \tag{4}$$

Table 1
RMSE computed for simulations obtained with different sets of $\varepsilon_{g\ max}$ and BR_{ini} values

Parameter/initial condition		RMSE	
ε_{gmax} (g DM MJ^{-1})	BR_{ini} (g DM m^{-2})	B_{ag} (g DM m^{-2})	NDVI
5.3	300	29.8	0.112
5.3	600	23.4	0.098
5.3	900	23.1	0.094
6.3	300	20.4	0.069
6.3	600	14.0	0.058
6.3	900	17.3	0.058
7.3	300	12.4	0.039
7.3	600	9.5	0.041
7.3	900	18.9	0.053
8.3	300	19.2	0.068
8.3	600	21.8	0.076
8.3	900	30.5	0.089

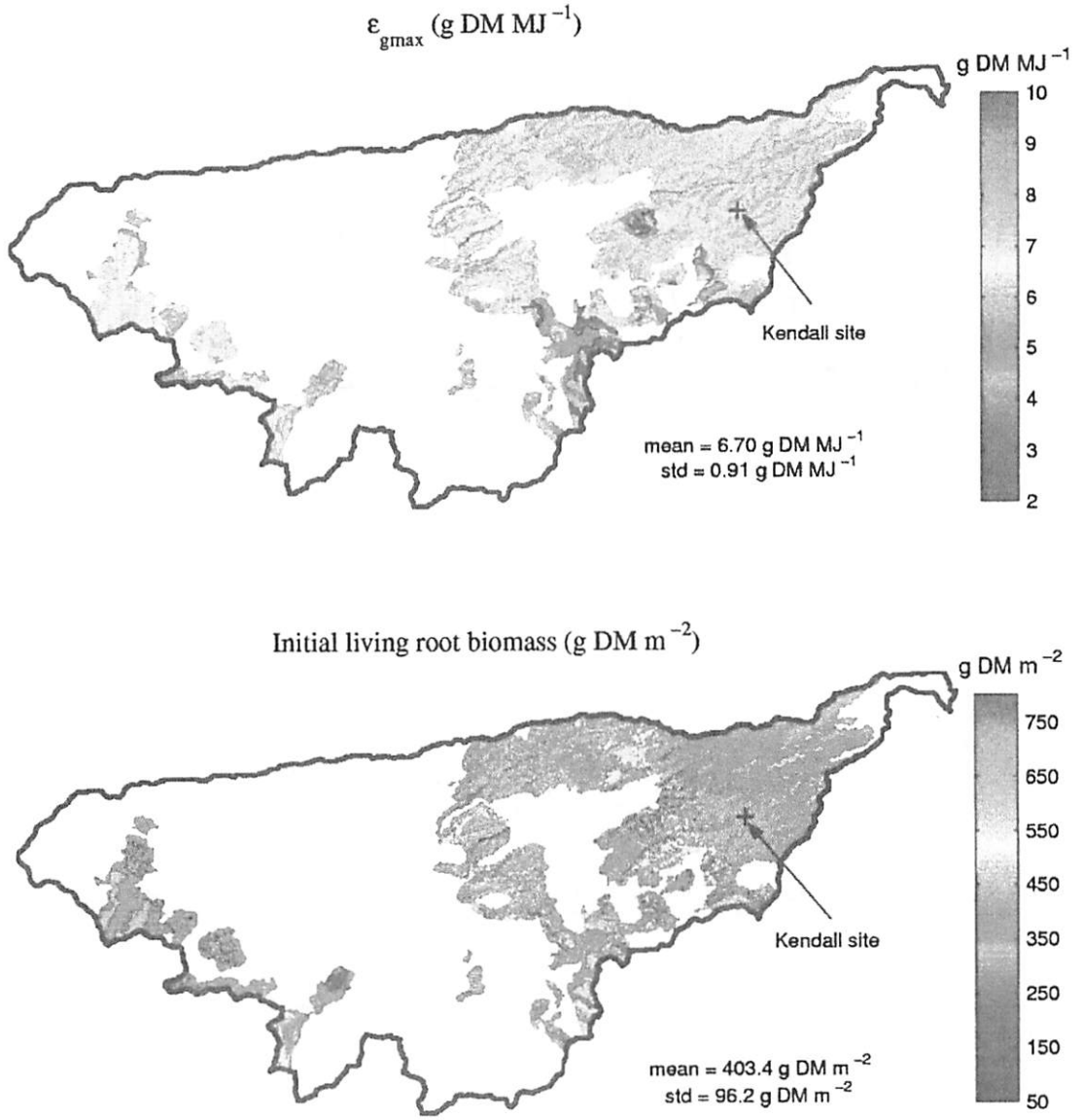

Fig. 5. Maps of maximum light use efficiency (ε_{gmax}) and initial living root biomass (BR_{ini}) obtained by model calibration (std is the standard deviation).

where $T(\theta)$ is the gap fraction in the direction θ, $\lambda(\theta)$ is the Markov parameter (or leaf dispersion parameter; Nilson, 1971), and $k(\theta)$ is the extinction coefficient (for a canopy characterized by a random leaf dispersion). The Markov parameter, $\lambda(\theta)$, equals 1 if leaves are randomly dispersed, but is less than 1 for clumped canopies (e.g., Baldocchi & Collineau, 1994; Kucharick, Norman, & Gower, 1999; Nilson, 1971). For sparse, clumped canopies, $\lambda(\theta)$, is expressed as (Kuusk, 1995a) (Eq. (5)):

$$\lambda(\theta) = 1 - (1 - \lambda_z)\frac{1 - \exp[-a\tan(\theta)]}{a\tan(\theta)}, \quad (5)$$

where λ_z is the dispersion parameter in the vertical direction ($\lambda_z = \lambda(0)$) and a is a canopy structure dependent parameter (Kuusk, 1995a).

Once the gap fractions are simulated, diffuse fluxes of shortwave radiation are computed in the MCCR model using a four-stream approximation (similar to the SAIL model (Verhoef, 1984)), while the single scattering is computed following the Nilson–Kuusk model (Kuusk, 1995b; Nilson & Kuusk, 1989), which accounts for specular reflection by leaves and canopy hot-spot. The leaf angle distribution (LAD) is described by an elliptical distribution and leaf optical properties from 400 to 2500 nm are computed from leaf biochemistry and structure using the PROSPECT model (Jacquemoud & Baret, 1990; Jacquemoud et al., 1996). In this study, the functions from Price (1990) used in the original version of the MCCR model to describe soil spectral and bidirectional properties have been replaced by the SOILSPECT model (Jacquemoud, Baret, & Hanocq, 1992).

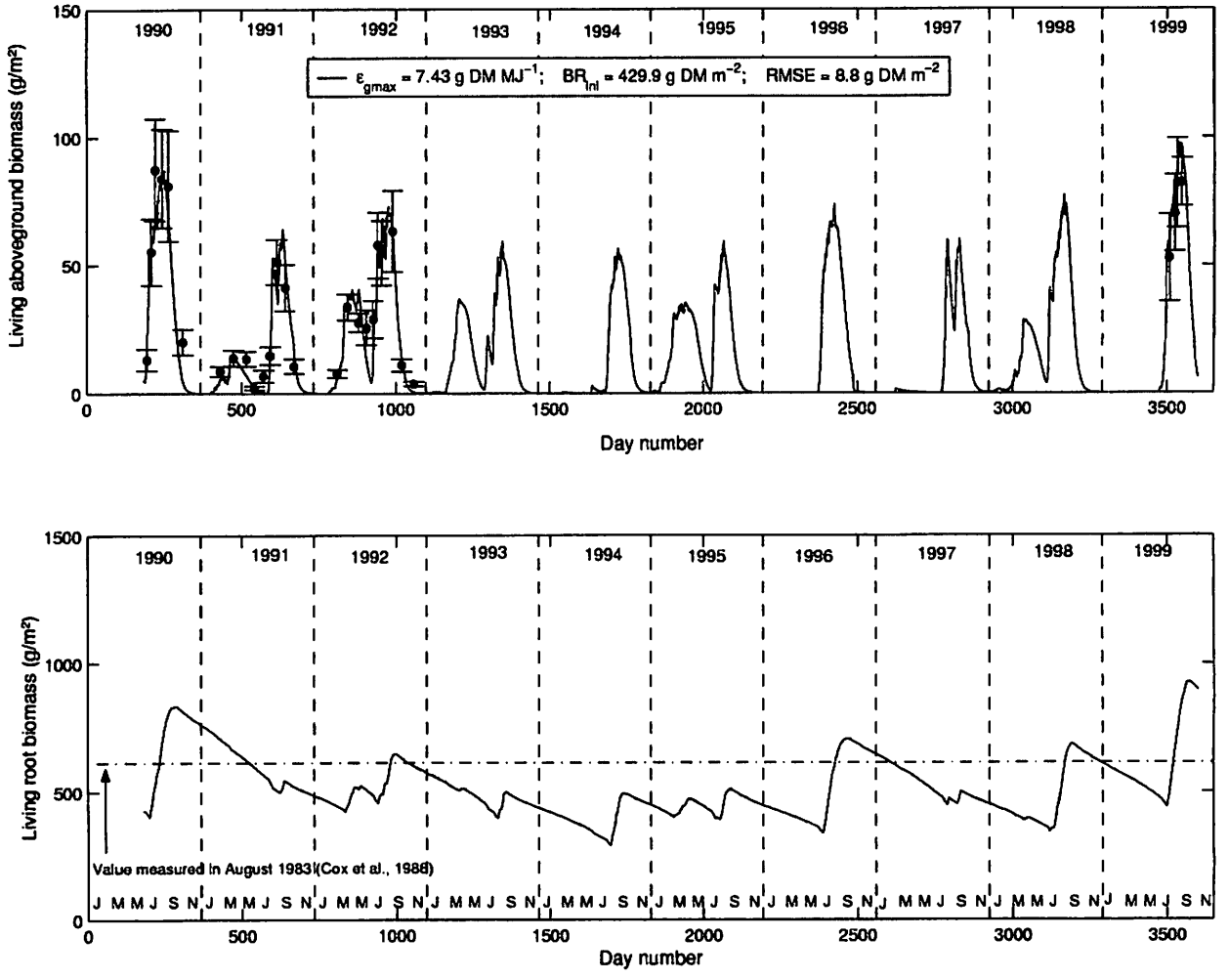

Fig. 6. Simulation results obtained at the Kendall site after model calibration using TM and ETM+ images (continuous lines). The retrieved values of ε_{gmax} and BR_{ini} are indicated on the figure. In the top graph, solid circles with error bars show aboveground biomass measurements. In the bottom graph, the horizontal broken line show the value of root biomass measured by Cox et al. (1986) in August 1983.

The MCCR model was linked with the plant growth model through the simulated green LAI. The parameters used to compute the angular course of the Markov parameter and the LAD were derived from extensive measurements of canopy structure and gap fractions on various sites in northern Mexico and southeast Arizona (Nouvellon, Bégué, et al., 2000). PROSPECT's parameters were estimated from model inversion against published data of leaf reflectance and transmittance (Asner, Wessman, Schimel, & Archer, 1998). SOILSPECT's parameters were obtained by model inversion using bidirectional reflectances measured over bare soils at the Kendall site, and were assumed constant for the whole TM images except the simple scattering albedos that were inverted for each TM band (in the visible) from pixel reflectances of images obtained during the dry season, corrected from atmospheric effects (as described below).

For canopy reflectance simulations, geometric configurations (sun/view zenith angles) were identical to corresponding satellite measurements. Reflectances in red and NIR TM and ETM+ bands were calculated from the simulated spectral reflectances (from 400 to 2500 nm with a 4-nm spectral resolution) using the spectral response function of the TM and ETM+ sensors (Eq. (6)):

$$\rho_c(\theta_s, \theta_v, \psi_{sv}) = \frac{\int_\lambda \rho(\lambda, \theta_s, \theta_v, \psi_{sv}) S_c(\lambda)}{\int_\lambda S_c(\lambda)}, \quad (6)$$

where $\rho(\lambda, \theta_s, \theta_v, \psi_{sv})$ is the canopy reflectance at wavelength λ; $\rho_c(\theta_s, \theta_v, \psi_{sv})$ is the canopy reflectance for channel c (red or NIR); θ_v, θ_s, and ψ_{sv} are the sensor view zenith angle, solar zenith angle, and the relative azimuth angle at the time of the measurements; and $S_c(\lambda)$ is the sensor spectral response function for wavelength λ in the channel c.

From reflectances simulated in the red and NIR TM and ETM+ bands, normalized difference vegetation index

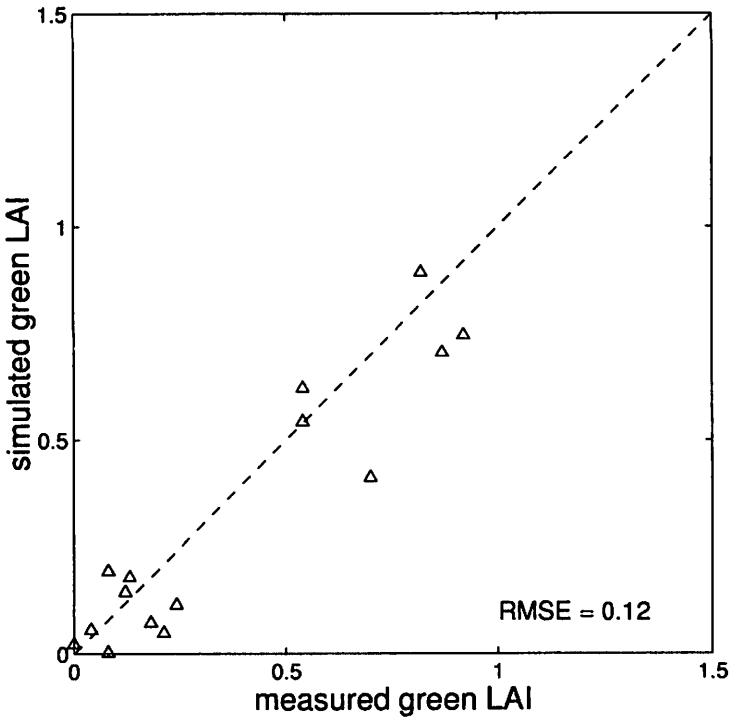

Fig. 7. Comparison of the GLAI simulated after model calibration and the GLAI measured at Kendall site.

(NDVI) were computed based on the well-known equation (Eq. (7)):

$$\mathrm{NDVI}_{\mathrm{sim}}(\theta_s, \theta_v, \psi_{sv}) = \frac{\rho_{\mathrm{NIR}}(\theta_s, \theta_v, \psi_{sv}) - \rho_{Red}(\theta_s, \theta_v, \psi_{sv})}{\rho_{\mathrm{NIR}}(\theta_s, \theta_v, \psi_{sv}) + \rho_{Red}(\theta_s, \theta_v, \psi_{sv})}, \quad (7)$$

where $\mathrm{NDVI}_{\mathrm{sim}}(\theta_s, \theta_v, \Psi_{sv})$ is the NDVI simulated by the combined EM-RTM at the time of the satellite overpass.

4. Model application and calibration

The model was applied on the grassland areas of the WGEW (selected from the vegetation map) using soil texture parameters provided by the soil map, and daily meteorological data (rainfall, solar radiation, maximum and minimum air temperature and relative humidity, wind speed) measured at the Kendall site from June 1990 through August 1999 (Fig. 2). The maximum distance between grassland pixels and the Kendall meteorological station was about 18 km, and the mean distance was about 5 km. This is typically the scale where the surface can be characterized with a disorganized or microscale heterogeneity for which the atmospheric boundary layer responds only to the composite surface structure. Therefore, the atmospheric forcing parameters can be assumed to be constant over the entire landscape (Chehbouni, Njoku, Lhomme, & Kerr, 1995). Additionally, the analysis of historical precipitation data from the WGEW performed by Nichols, Lane, Asce, and Manetsch (1993) has shown that daily precipitation was much less variable in space than storm precipitation. The correlation coefficients between daily precipitation amounts from two locations separated by 5 km were about .9 and .6 for winter and summer precipitation, respectively, considering only days of measurable precipitation. These coefficients increase with the time of integration, e.g., for weekly or seasonal total precipitation (Nichols et al., 1993).

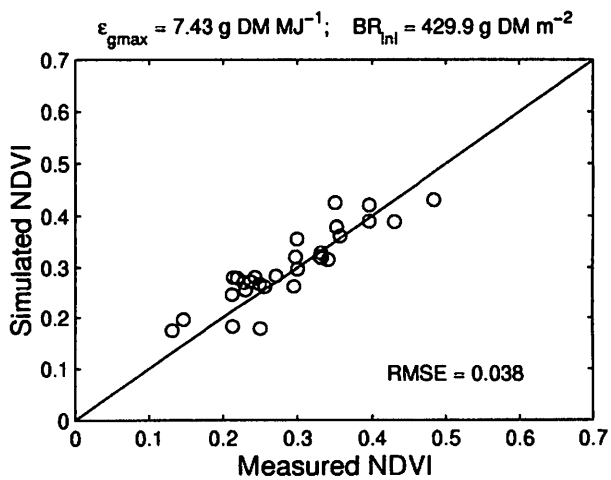

Fig. 8. Comparison of the NDVI simulated after model calibration and the NDVI measured by TM and ETM+ sensors.

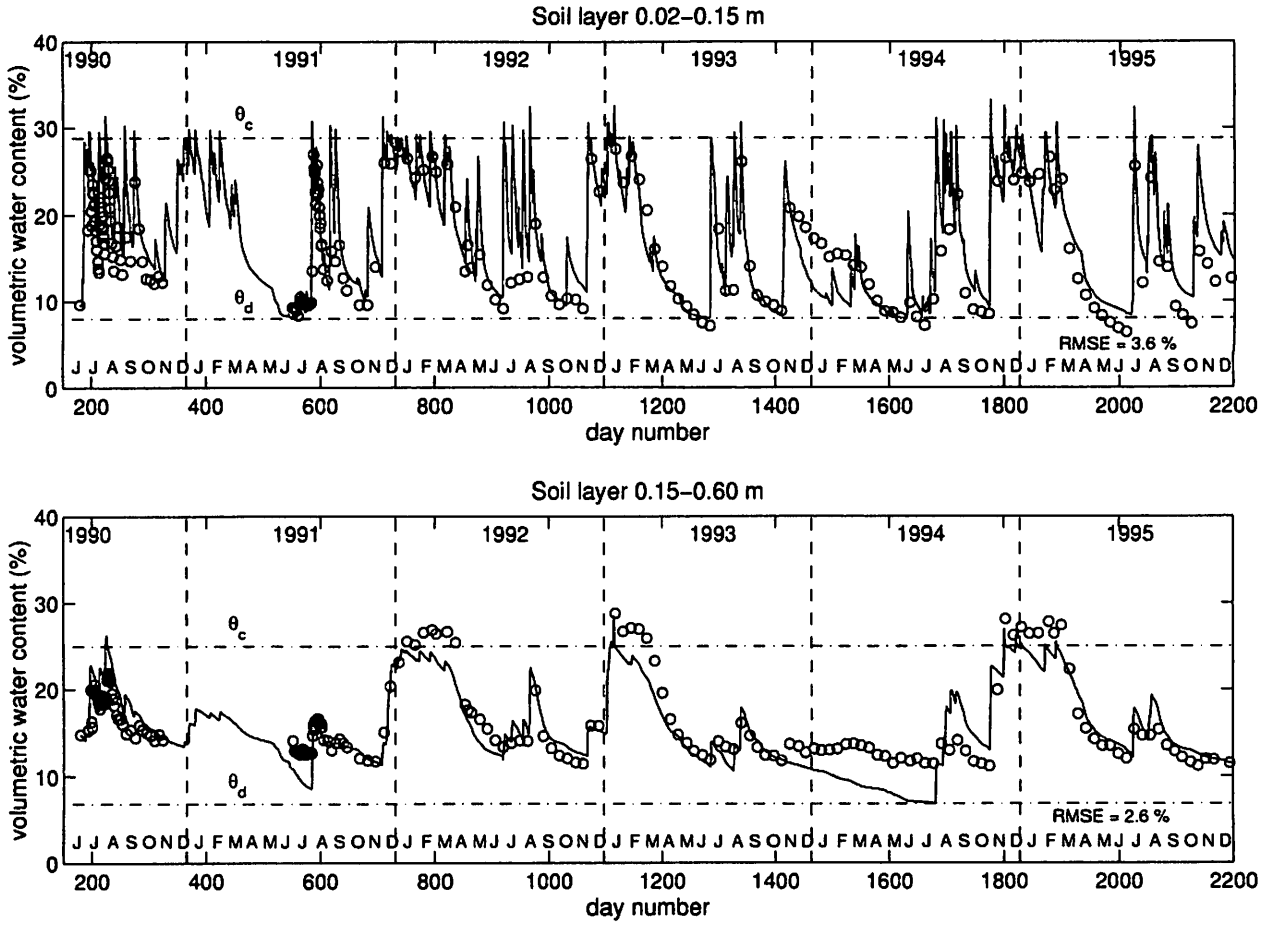

Fig. 9. Volumetric soil water content of layers 0.02–0.15 and 0.15–0.60 m. Solid lines refer to simulations and circles refer to measurements. Broken lines show field capacity and soil water content at air dryness.

Image corrections for atmospheric effects were not based on atmospheric RTM (e.g., Rahman & Dedieu, 1994; Tanré et al., 1990) since required information about the atmospheric conditions were unknown for the majority of the images. Instead, the refine empirical line (REL) approach (Moran et al., this issue) was used to convert image digital number (dn) to surface reflectance factor, with an estimated accuracy of 0.01 for red and NIR TM and ETM+ bands (Moran et al., this issue).

NDVI simulated by the combined EM-RTM were compared to NDVI calculated from reflectances measured by TM and ETM+ sensors and corrected for atmospheric effects ($NDVI_{obs}$). Spatially unknown initial conditions and parameters were estimated using an iterative procedure based on the simplex method (Nelder & Mead, 1965) that minimized the cost function E_{NDVI} defined as (Eq. (8)):

$$E_{NDVI} = \frac{1}{n_{obs}} \sum_{i=1}^{n_{obs}} (NDVI_{sim} - NDVI_{obs})^2, \quad (8)$$

where n_{obs} is the number of observations (images) and $NDVI_{sim}$ and $NDVI_{obs}$ are the simulated and observed NDVI, respectively.

Those parameters and initial conditions chosen to be reparameterized/reinitialized were those (1) to which the process model was highly sensitive, so that any change of their values greatly impacts the aboveground biomass from which the leaf area index (LAI, used as input to the RTM) is derived; (2) which are spatially variable; and (3) which are difficult to obtain by direct measurement at the watershed scale. Following a previous sensitivity analysis, and taking into account the above criteria, initial living root biomass, BR_{ini}, and maximum light use efficiency, ε_{gmax} (see Eq. (3)) were selected for the remotely sensed based calibration. For C_4 grasses, most of the published values of ε_{gmax} range between 5 and 9 g DM MJ^{-1} (e.g., Charles-Edwards, Doley, & Rimmington, 1986; Ehleringer & Pearcy, 1983; Goetz & Prince, 1999; Hanan, Prince, & Bégué, 1997; Prince & Goward, 1995; Saugier, 1992). The range of variation of ε_{gmax} may be even larger in natural environments such as WGEW, due to spatial variations of plant species composition and soil nutrient status. A wide range of values is also expected for BR_{ini}, which depends both on range conditions and on the time of the year when the simulations start. For short-grass ecosystems, published estimations of root biomass generally range between 200 and 1200 g DM m^{-2}

depending on site locations and conditions, time of the year, sampling schemes, and harvest methods (e.g., Cox et al., 1986; Dodd & Lauenroth, 1997; Hook, Lauenroth, & Burkes, 1994; Liang, Hazlett, & Lauenroth, 1989; Nouvellon, 1999; Parton, Singh, & Coleman, 1978; Sims & Singh, 1978; Sims, Singh, & Lauenroth, 1978; Singh & Coleman, 1975).

Applying the calibration procedure to every grassland pixel of the WGEW (or for small clusters of adjacent pixels) is feasible but has a high computational requirement. To minimize the time consumed by the application of the calibration procedure over the WGEW, we reduced the redundancy of surface conditions by classifying the 60,199 pixels into 25 distinct classes related to similar temporal profiles of NDVI. This was obtained with an unsupervised classification based on NDVI derived from the 29 TM and ETM+ images. This reduced the number of model calibrations to a maximum number of 600 possible combinations (25 NDVI classes by 24 soil classes).

5. Results

5.1. Model sensitivity to potential energy conversion efficiency and initial root biomass

A demonstration of model sensitivity to $\varepsilon_{g\ max}$ and BR_{ini} is presented in Figs. 3 and 4. On Fig. 3, daily courses of biomass obtained at the Kendall site for the 10-year period using two a-priori sets of possible values of ε_{gmax} and BR_{ini} were compared to aboveground biomass measured on this site from 1990 to 1999. The NDVI simulated by the combined EM-RTM for these two a-priori parameter sets were also compared to TM/ETM+ derived NDVI (mean values of NDVI of the cluster of pixels that includes the Kendall site; Fig. 4). The first set of a-priori values of ε_{gmax} and BR_{ini} resulted in overestimation of measured aboveground biomass (root mean square errors, RMSE of 21.8 g DM m^{-2}) and NDVI (RMSE of 0.076). Underestimation of biomass and NDVI resulted from the second set (RMSE of 20.4 g DM m^{-2} and 0.069, respectively). The RMSE values computed for other combinations of ε_{gmax} and BR_{ini} are reported in Table 1. The results show that model errors due to uncertain values of ε_{gmax} and BR_{ini} strongly propagate in the RTM resulting in sensitivity of NDVI to ε_{gmax} and BR_{ini}. The high RMSE obtained for some combinations of possible values of ε_{gmax} and BR_{ini} stress the importance of model calibration.

5.2. Calibration results

The maps of maximum light use efficiency (ε_{gmax}) and initial living root biomass (BR_{ini}) obtained after model calibration are shown in Fig. 5. Retrieved ε_{gmax} exhibited

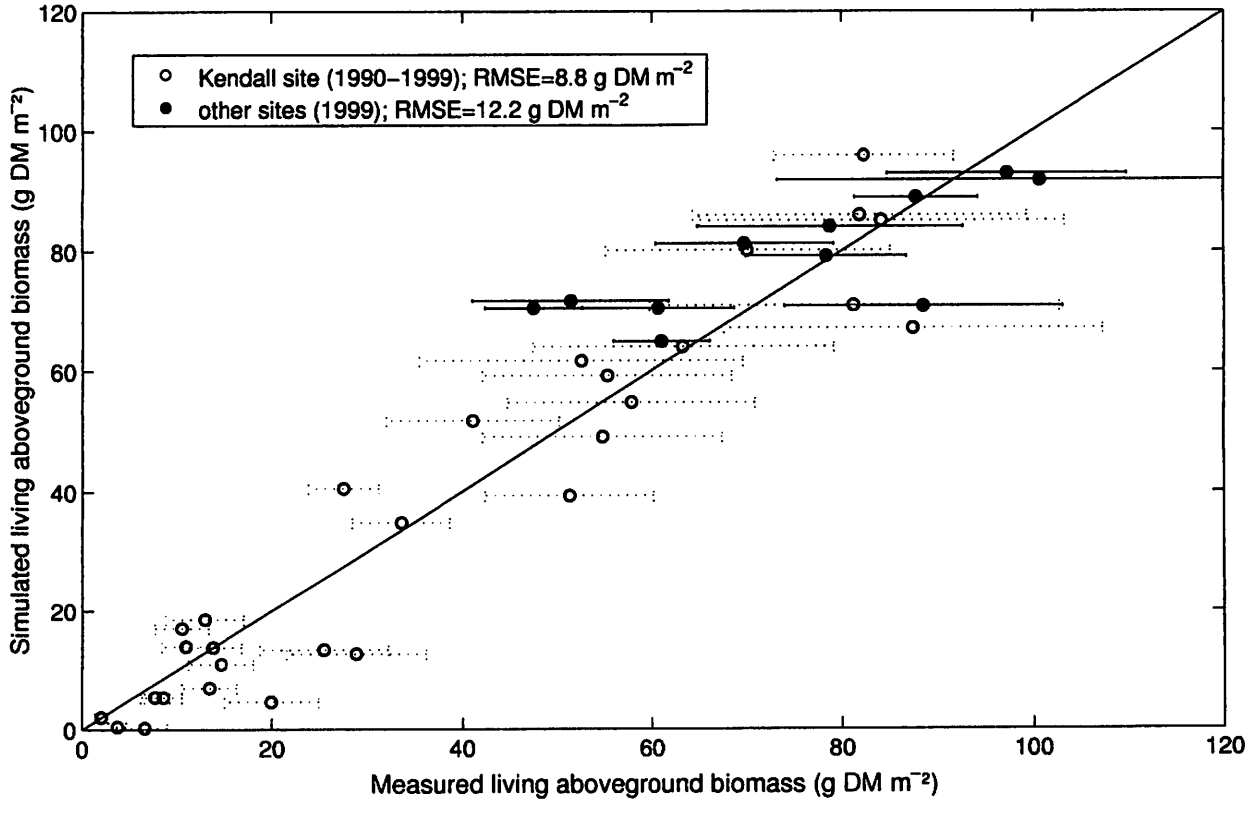

Fig. 10. Comparison of simulated and measured living aboveground biomass.

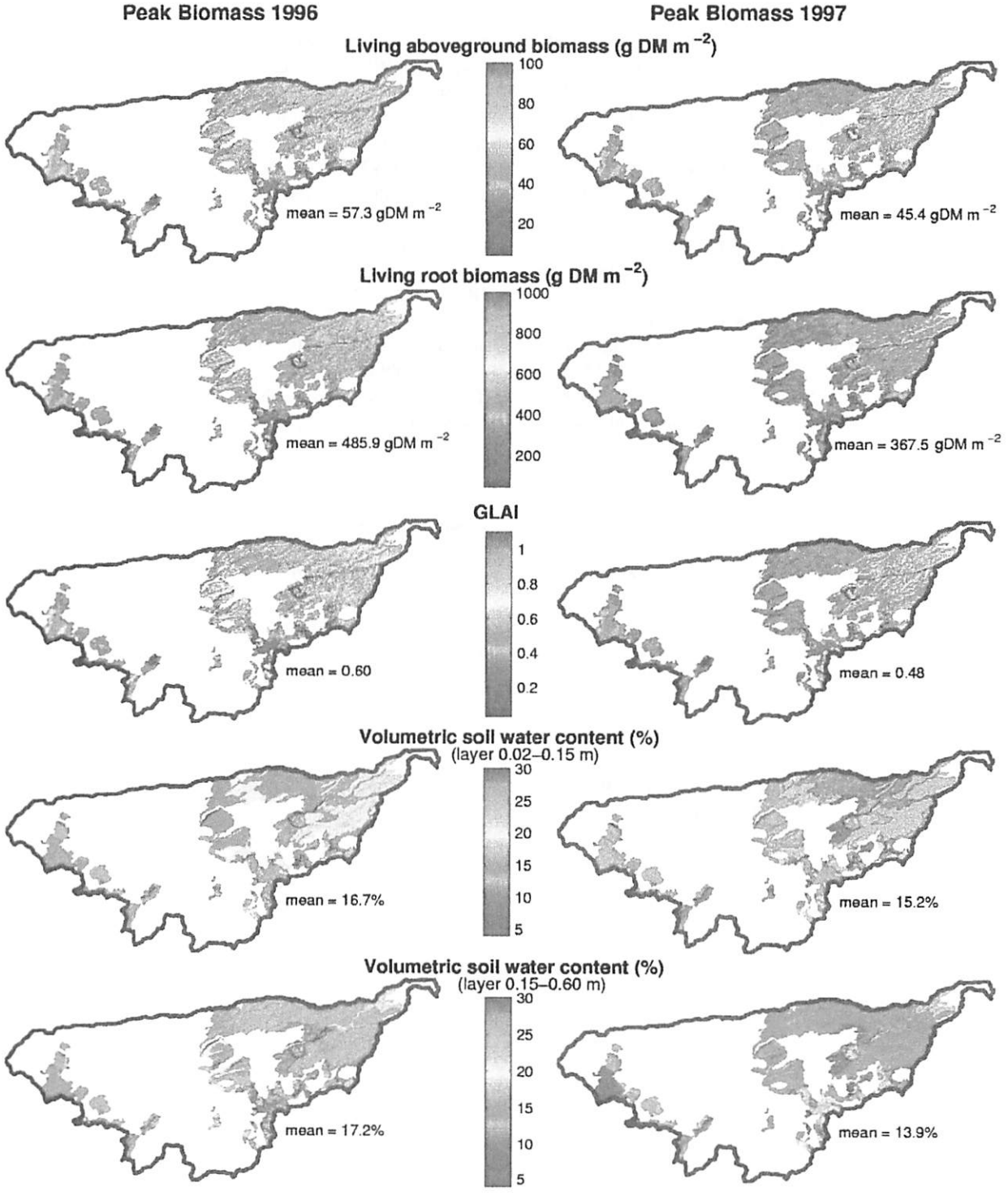

Fig. 11. Maps of simulated (1) living aboveground biomass, (2) living belowground biomass, (3) GLAI, (4) volumetric soil water content of layers 0.02–0.15 m, and (5) volumetric soil water content of layers 0.15–0.60 m on the WGEW at peak biomass 1996 and 1997.

high spatial variation, with values ranging from 2.1 up to 11.5 g DM MJ^{-1} for the most productive areas. Most of these were found in the range of values given in the literature. About 91% of the values ranged between 5 and 9 g DM MJ^{-1}, and 95% between 4.3 and 9.6 g DM MJ^{-1}. The unexpected lowest values (2.1 g DM MJ^{-1}) occurred in pixels that partially cover road tracks or former surface mine areas. The mean value of retrieved ε_{gmax} was about

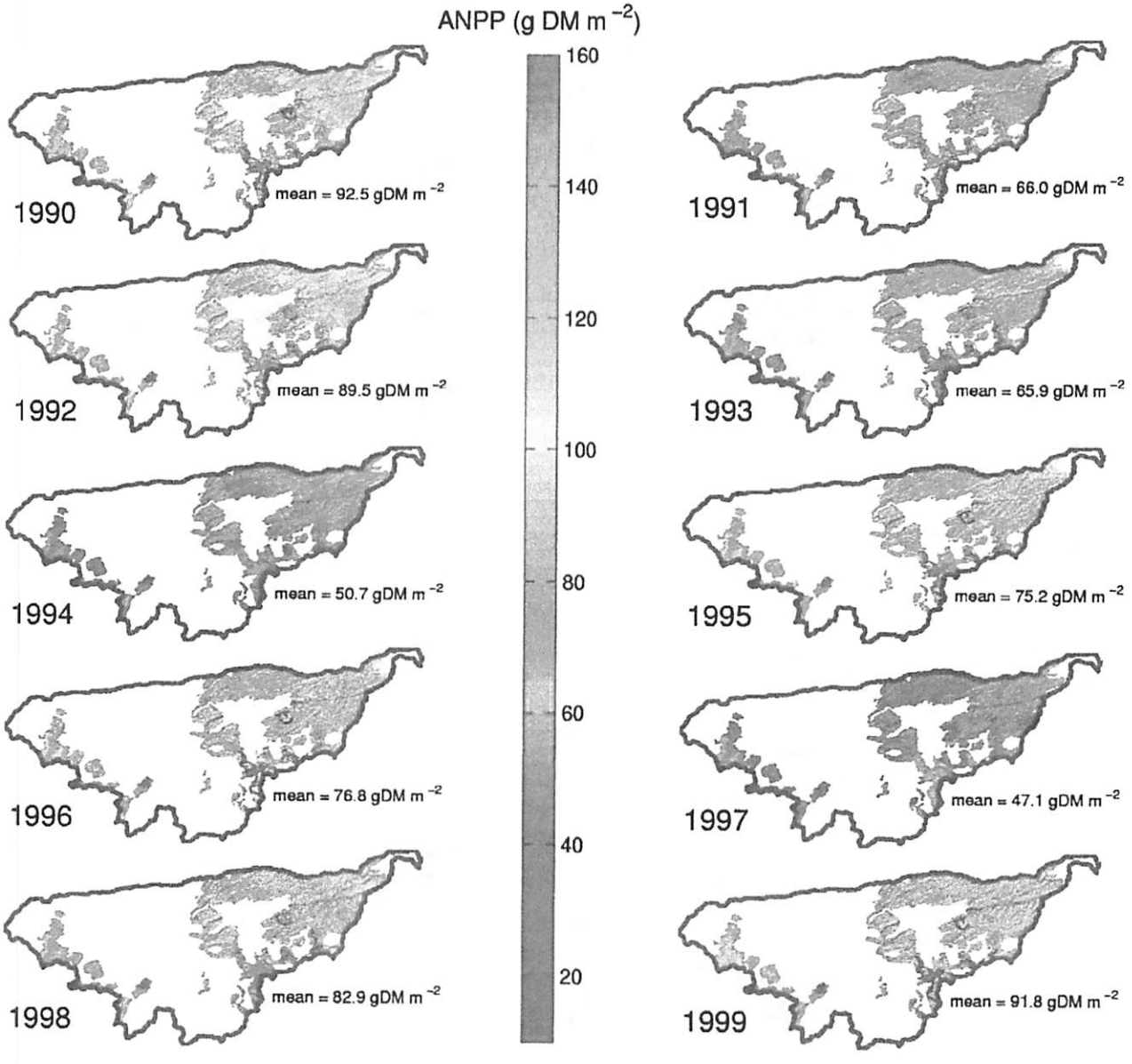

Fig. 12. Maps of simulated ANPP from 1990 to 1999.

6.7 g DM MJ $^{-1}$. As a comparison, the values given in Prince and Goward (1995) and Charles-Edwards et al. (1986) for maximum conversion efficiency for C_4 grasses are 6.9 and 8 g DM MJ $^{-1}$, respectively.

Similar to ε_{gmax}, estimated values of initial living root biomass (BR_{ini}) exhibited high-spatial variation, from 35 up to 893 g DM m $^{-2}$, with their minimum values obtained for the pixels that had the lowest ε_{gmax}. All these values were found in a biologically meaningful range, similar to the values given in the literature for such ecosystems (e.g., Cox et al., 1986; Nouvellon, 1999; Sims et al., 1978). About 91% of calculated values ranged between 200 and 600 g DM m $^{-2}$. The mean value was about 403 g DM m $^{-2}$. As a comparison, the living root biomass measured by Nouvellon (1999) on several short-grass sites in northern Sonora (at about 50 km south to the WGEW) in July 1997 (before the monsoon growing season) ranged between 376 and 526 g DM m $^{-2}$.

5.3. Simulation results after model calibration

The Kendall site had estimated values of ε_{gmax} and BR_{ini} of 7.43 g DM MJ $^{-1}$ and 429.9 g DM m $^{-2}$, respectively (Fig. 5). Biomass and GLAI simulated at the Kendall site after model calibration (with estimated values of ε_{gmax} and BR_{ini}), on a daily basis over the 10-year simulation period were compared to field measurements (Figs. 6 and 7). The NDVI simulated by the calibrated EM-RTM were also compared to the NDVI derived from satellite measurements (Fig. 8). A comparison of soil water content in layers

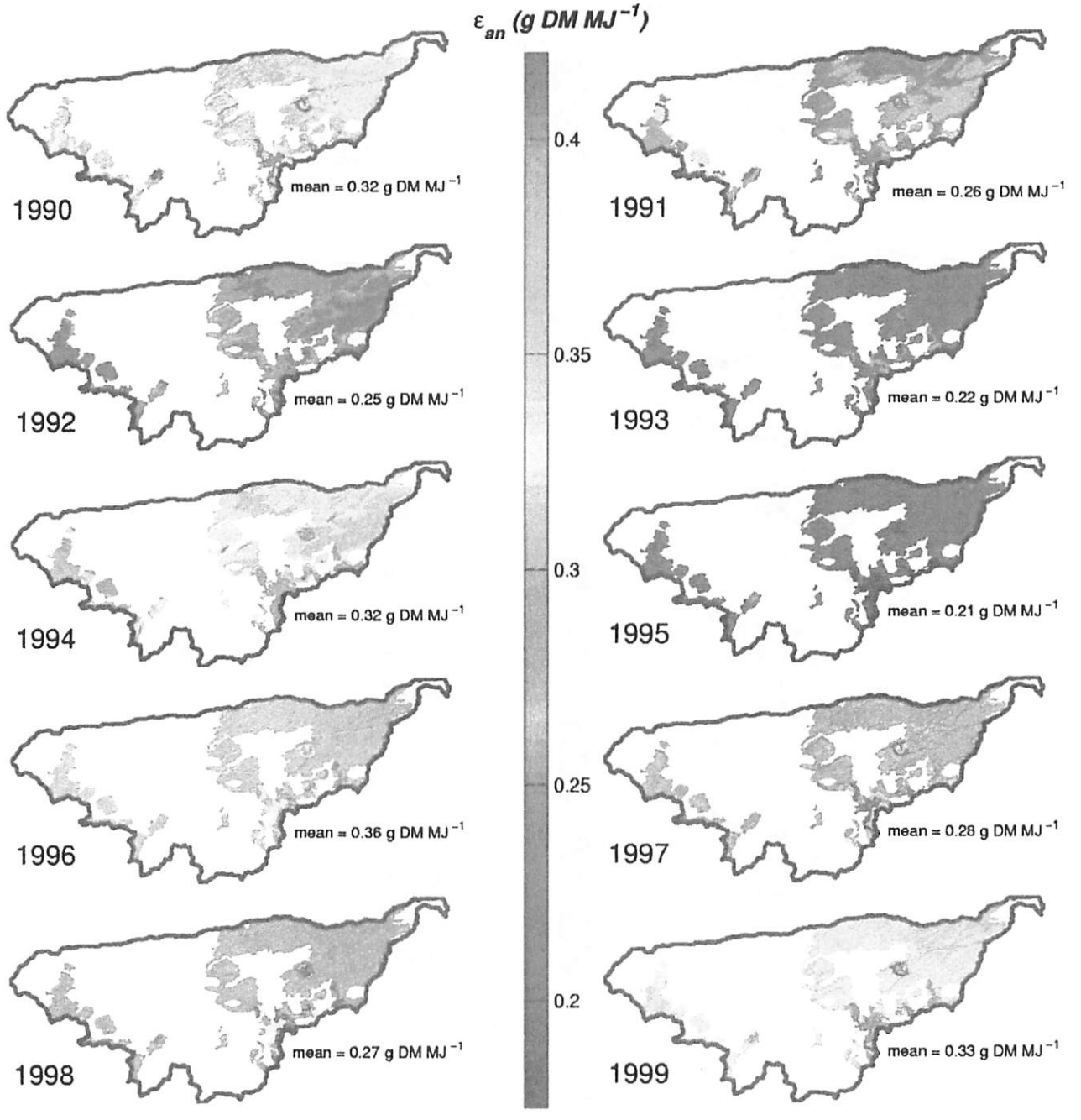

Fig. 13. Maps of calculated aboveground net production (radiation-use) efficiencies, ε_{an}, from 1990 to 1999.

0.02–0.15 and 0.15–0.60 m simulated by the calibrated model and measured at the Kendall site (TDR probes) from June 1990 through December 1995 is also presented (Fig. 9).

The results show that after calibration, simulated aboveground biomass and GLAI were in good agreement with measurements, with RMSE of only 8.8 g DM m^{-2} and 0.12, respectively (Figs. 6 and 7). The RMSE for living aboveground biomass and NDVI are about two times less than the RMSE obtained before calibration with the two a-priori sets of ε_{gmax} and BR_{ini} values (Figs. 3 and 4). For most years, depending on the rainfall distribution, plant growth pattern was bimodal. There was limited plant growth in the spring when temperatures and soil condition were favorable (spring growth did not occur for years 1994, 1997, and 1999 due to insufficient late winter and spring precipitation). In May and June, most of the vegetation dries up due to water limitations. The most significant growth then occurs during the summer (July–October) season.

Over the 10-year period, no data were available to validate root biomass simulations. Simulated living root

biomass was compared to the value measured by Cox et al. (1986) in August 1983 at the Kendall site. Root biomass decreases between consecutive growing seasons due to respiration and senescence. This decrease is accelerated during the onset of vegetation growth in spring and summer due to translocation of carbohydrates from root to young shoots. After shoot development, when the amount of photoassimilated carbon allocated from the shoots to roots exceed root respiration and senescence, root biomass increases, and reaches its maximum value at the end of the summer growing season (late September/early October). This dynamic is similar to those described in other studies for short-grass ecosystems (e.g., Bachelet et al., 1989; Detling et al., 1979).

Comparisons of simulated and measured soil water contents show the ability of the calibrated model to adequately reproduce the time course of soil water (Fig. 9). The RMSE was about 3.6% for layer 0.02–0.15 m and 2.6% for layer 0.15–0.60 m. Model estimates of field capacity, θ_c (defined as the soil water content at −0.033 MPa) and soil water content at air dryness, θ_d (defined as the soil water content at −150 MPa) are drawn for each soil layer (horizontal lines). Their accuracy depends on soil map accuracy. For the deeper soil layer (0.15–0.60 m), θ_c and θ_d are slightly underestimated, as suggested by the model underestimations observed for the highest soil water contents (e.g., February 1992) and for the lowest soil water contents (e.g., June 1994).

The biomass measured at other sites during 1999 summer growing season were also used for further model evaluation. Living aboveground biomass simulated at these sites by the calibrated model were compared to field measurements (Fig. 10). Good agreement was obtained between simulations and measurements. At these sites, the accuracy was of the same order as the accuracy obtained at the Kendall site from 1990 through 1999.

Maps of living aboveground biomass, living belowground biomass, GLAI, and soil moisture obtained at peak biomass of two contrasted summer growing seasons (1996 and 1997) are presented in Fig. 11. Living aboveground biomass simulated at peak biomass was higher in 1996 than in 1997 (the average was 57.3 g DM m^{-2} in 1996 and 45.4 g DM m^{-2} in 1997). Spatial variations, however, were found to be even larger. A similar pattern was found for belowground biomass and GLAI.

At peak biomass, mean GLAI was about 0.60 in 1996 and 0.48 in 1997 (Fig. 11). GLAI varied by more than 20 times from the less productive areas to the more productive areas. For comparison, the GLAI measured by Knight (1973), Hazlett (1992), and Nouvellon, Bégué, et al. (2000) near peak biomass on several short-grass ecosystem sites and for different years ranged from 0.1 to 1.7.

At peak biomass, most of the soil water in the layer 0.02–0.15 m had been lost through evapotranspiration, and the spatial variability of soil moisture was closely related to the spatial variability of soil texture (Fig. 11 vs. Fig. 2). For each soil class, soil moisture in the layer 0.02–0.15 m was negatively correlated to GLAI, due to the high efficiency of perennial grasses to extract soil water and recycle it to the atmosphere.

The ANPP simulated for the ten years is presented in Fig. 12. The results show both high spatial and inter-annual variations. The lowest mean values were obtained in 1997 and 1994 (47.1 and 50.7 g DM m^{-2}) and the highest were obtained in 1990 and 1999 (92.5 and 91.8 g DM m^{-2}). The ANPP for the most productive years was therefore twice as high as the ANPP of the less productive ones. The aboveground net production (radiation-use) efficiencies (ε_{an}), calculated on an annual basis (from simulated ANPP and APAR; see Nouvellon, Lo Seen, et al., 2000) are presented in Fig. 13. The spatially averaged ε_{an} was the lowest in 1995 (0.21 g DM MJ^{-1}) and the highest in 1996 (0.36 g DM MJ^{-1}). For the most water-limited years (e.g., 1997), the spatial pattern of ε_{an} reflects approximately the spatial pattern of soil texture. Over the whole 10-year period, the mean ε_{an} was about 0.28 g DM MJ^{-1}.

6. Discussion

The overall results indicate that this approach, which combines grassland modeling and remote sensing, may prove an efficient tool for accurate, multiyear simulation and mapping of key variables for grassland management (e.g., aboveground biomass) or for ecological and climatological studies (e.g., LAI, gross and net primary productivities, soil moisture, evapotranspiration). After model calibration using time series of TM and ETM+ images, aboveground biomass, soil water content, and GLAI were simulated with good accuracy (low RMSE).

The simulated ANPP were found to be highly variable both spatially and temporally, with mean annual values ranging from 47 to 92 g DM m^{-2}. For short-grass ecosystems, most of ANPP values reported in the literature range from 40 to 150 g DM m^{-2} $year^{-1}$ (e.g., Epstein, Burke, & Lauenroth, 1999; Epstein, Lauenroth, Burke, & Coffin, 1998; Lauenroth & Sala, 1992; Milchunas & Lauenroth, 1992; Sims & Singh, 1978). Several studies have shown that for semiarid perennial grassland ecosystems, ANPP depends not only on the rainfall pattern of the current growing season, but also on those of the previous years due to the storage of carbohydrates in the root system (e.g., Cable, 1975; Webb, Szarek, Lauenroth, Kinerson, & Smith, 1978). There is a carryover of productivity potential from previous years (Lauenroth & Sala, 1992; Webb et al., 1978), which stress the importance of continuous, multiyear simulations, as done in this study. This 'carryover' effect was well simulated by the model, and partially explained the low ANPP of 1994, and the high productivity obtained in 1999 (the second year of 2 consecutive years of favorable precipitation; see Figs. 6 and 12).

Radiation use efficiencies (RUE) and water use efficiencies (WUE) are widely used by ecologists to analyze and compare ecosystems of diverse environments. The concept of RUE has also been increasingly used to provide regional or global estimations of ecosystem gross and net primary productivity from remotely sensed estimates of APAR (e.g., Gower, Kucharick, & Norman, 1999; Prince, 1991; Prince & Goward, 1995; Ruimy, Saugier, & Dedieu, 1994). The accuracy of RUE models, however, depends on accurate estimations of the production (radiation-use) efficiencies (ε), which are known to vary according to environmental conditions, phenology, and species composition (Goetz & Prince, 1998). The spatially averaged ε_{an}, computed on an annual basis, ranged from 0.21 to 0.36 g DM MJ^{-1}. Over the whole 10-year period, the mean ε_{an} was about 0.28 g DM MJ^{-1}. For comparison, the 4-year average values published by Paruelo, Epstein, Lauenroth, and Burke (1997) for several shortgrass steppes ranged approximately between 0.1 (0.25) and 0.15 g C MJ^{-1} (0.37 g DM MJ^{-1}). These values are about two to three-fold less than those found for mixed-grass or tall grass ecosystems (e.g., Paruelo et al., 1997) or semiarid annual grasslands (e.g., Hanan, Prince, & Bégué, 1995; Mougin et al., 1995), which are known to allocate a lower proportion of assimilate to the belowground compartment (e.g., Ryle, 1970).

It is of interest to observe that the 'carry over effect' previously described for ANPP and reported by many authors (e.g., Cable, 1975; Lauenroth & Sala, 1992; Webb et al., 1978) is even more apparent on ε_{an} than on ANPP (e.g., the lowest ε_{an} was obtained in 1995 after 2 low-productive years). This has important implications for applications based on RUE models, since the interannual variations of the required efficiency could not be simply predicted from correcting factors that account only for the climatic condition of the current year. By contrast, assimilating satellite images in an EM, as done in this study, allows continuous, multiyear simulations of the carbon budget, which correctly reproduce the influence of rainfall of previous years on productivity of a given year.

One potential application of the present methodology is the integration into an operational grassland management system. However, many aspects of the procedure should be improved for that integration to be successful. For this reason, a number of studies have already been initiated to:

(1) Test more robust and low time-consuming calibration procedures, for example, those based on extended and nonlinear Kalman-filtering. This latter procedure, in contrast to the simplex method, allows considerations of both measurement and model errors and provides robust estimations of values and uncertainties of parameters and state variables (e.g., Cahill, Ungaro, Parlange, Mata, & Nielsen, 1999; Rambal, Romane, & Aguilar-Martin, 1977).
(2) Use in synergy optical, thermal, and microwave remotely sensed data. While optical and microwave data can give information about the amount and structure of vegetation, thermal as well as microwave data can be used to assess its water status (e.g., Moran et al., 1996, 1997). In addition, thermal data inform about processes, which occur at time scales shorter than the day. Therefore, in order to take full account of the different types of remotely sensed data, the water and energy budgets are being modeled with an hourly time step (e.g., Lo Seen et al., 1997; Nouvellon, Moran, et al., 2000). When used together, this should result in a tighter control of the model simulations and improvement in the estimation of terms of the water budget.
(3) Address the problem of how meteorological data obtained at discrete locations can be used on a spatially distributed basis. In our case, spatialization of meteorological data has not been necessary due to the limited extent of the study area. However, application to larger areas will be limited by the lack of continuous fields of meteorological variables on a daily time step. An approach is currently being tested to retrieve spatially distributed meteorological data at a fine 4-km resolution from a mesoscale meteorological model (Moran, Nouvellon, Bryant, & Ni, 2000; Toth, 1997).
(4) Relate long term plant production and resource use efficiencies (LUE and WUE) to long-term runoff or erosion. This is being done by coupling the EM with a runoff model (the KINEROS model (Smith, Goodrich, Woolhiser, & Unkrich, 1995)) together with a Digital Elevation Model (DEM). It is expected that information on this relation may give insights on the mechanisms of landscape degradation. The objective is to build a computationally efficient tool capable of real-time simulations of plant growth and hydrologic processes, as well as simulations of land management scenarios.

7. Conclusions

In this study, a coupled EM-RTM was run on a spatially distributed basis with assimilation of a 10-year time series of Landsat TM and ETM+ data. Satellite derived NDVI was used to control the simulation of the coupled model through a calibration procedure, which estimated two important spatially variable initial conditions and model parameters. Simulations for an area of about 150 km^2 around the Kendall site, continuous over ten years, gave consistent results when compared with field measurements of biomass, LAI, and soil moisture. These results suggest that the approach, using modeling with remote sensing, may prove more useful in grassland management than either in isolation.

An important feature of this method, for scaling up grassland productivity and water budget, is the ability to perform continuous multiyear simulations which correctly

reproduce the influence of rainfall of previous years on productivity of a given year. In this way, it was possible to map key ecological variables like LAI, soil water content and biomass for any day during the 10-year period as well as to follow their time courses. The overall performance of the model in the variety of situations met, both in space and time, indicate that this method is adequate. Our results have also pointed out that for short-grass ecosystems, due to time variation of RUE, the accuracy of approaches based on the time-integral of spectral vegetation indices (SVI) would be limited, further supporting our modeling approach.

The promising results obtained in this study, together with the improvements expected with ongoing work, suggest that an approach based on coupling an EM and high resolution multispectral satellite images like from the TM and ETM+ sensors could result in accurate and operational tools to provide spatially distributed information about vegetation and soil conditions for day-to-day grassland management.

Acknowledgments

This research activity has been funded by Landsat7 (NASA-S-41396-F) project and was carried out in the framework of SALSA-Global change research program (NASA grant W-18, 997), Monsoon '90 (IDP-88-086) and VEGETATION (58-5344-6-F806 95/CNES/0403). The CIRAD grant for Y. Nouvellon during his thesis research is gratefully acknowledged. The authors wish to thank Dr. Kuusk for providing the MCCR model, Dr. Jacquemoud for providing the SOILSPECT and PROSPECT models, and two anonymous reviewers for their helpful comments on the manuscript.

References

Amer, S. A., Keefer, T. O., Weltz, M. A., Goodrich, D. C., & Bach, L. B. (1994). Soil moisture sensors for continuous monitoring. *Water Resources Bulletin, 30* (1), 69–83.

Asner, G. P., Wessman, C. A., Schimel, D. S., & Archer, S. (1998). Variability in leaf and litter optical properties: implications for BRDF model inversions using AVHRR, MODIS, and MISR. *Remote Sensing of Environment, 63*, 243–257.

Bachelet, D., Hunt, H. W., & Detling, J. K. (1989). A simulation model of intraseasonal carbon and nitrogen dynamics of blue grama swards as influenced by above- and belowground grazing. *Ecological Modelling, 44*, 231–252.

Baldocchi, D., & Collineau, S. (1994). The physical nature of solar radiation in heterogeneous canopies: spatial and temporal attributes. In: M. M. Pearcy, & R. W. Pearcy (Eds.), *Exploitation of environmental heterogeneity by plants* (pp. 21–71). San Diego, CA, USA: Academic Press.

Bégué, A., Luquet, D., Dauzat, J., & Nouvellon, Y. (2001). Sensitivity of simulated optical properties of a semi-arid grassland to the accuracy of the 3D vegetation structure description – from SAIL model to ray-tracing technique. To be submitted to *Remote Sensing of Environment*.

Boote, K. J., Jones, J. W., & Pickering, N. B. (1996). Potential uses and limitations of crop models. *Agronomy Journal, 88*, 704–716.

Bouman, B. A. M. (1992). Linking physical remote sensing models with crop growth simulation models, applied for sugar beet. *International Journal of Remote Sensing, 14*, 2565–2581.

Breckenfeld, D. J., Svetlik, W. A., & McGuire, C. E. (1995). Soil survey of walnut gulch experimental watershed. US Department of Agriculture, Soil Conservation Service Special Report.

Brooks, R. H., & Corey, A. T. (1964). Hydraulic properties of porous media. Hydrology paper 3, Colorado State University, Fort Collins.

Burke, E. J., Gurney, R. J., Simmonds, L. P., & Jackson, T. J. (1997). Calibrating a soil water and energy budget model with remotely sensed data to obtain quantitative information about the soil. *Water Resources Research, 33* (7), 1689–1697.

Cable, D. R. (1975). Influence of precipitation on perennial grass production in the semidesert southwest. *Ecology, 56*, 981–986.

Cahill, A. T., Ungaro, F., Parlange, M. B., Mata, M., & Nielsen, D. R. (1999). Combined spatial and Kalman filter estimation of optimal soil hydraulic properties. *Water Resources Research, 35* (4), 1079–1088.

Camillo, P. J., O'Neil, P. E., & Gurney, R. J. (1986). Estimating soil hydraulic parameters using passive microwave data. *IEEE Transactions on Geoscience and Remote Sensing, 24* (6), 930–936.

Campbell, G. S. (1974). A simple method for determining unsaturated conductivity from moisture retention data. *Soil Science, 117*, 311–314.

Cayrol, P., Moulin, S., Kergoat, L., Dedieu, G., & Chehbouni, A. (2000). Calibrating a coupled SVAT/Vegetation growth model with remotely sensed reflectance and surface temperature. A case study for the HAPEX-Sahel grassland sites. *Journal of Applied Meteorology, 39*, 2452–2472.

Charles-Edwards, D. A., Doley, D., & Rimmington, G. M. (1986). *Modelling plant growth and development*. Orlando, FL: Academic Press.

Chehbouni, A. G., Njoku, E. G., Lhomme, J. P., & Kerr, Y. H. (1995). An approach for averaging surface temperature and surface fluxes over heterogeneous terrain. *Journal of Climate, 8* (5), 1386–1393.

Clevers, J. G. P., Büker, C., Van Leeuwen, H. J. C., & Bouman, B. A. M. (1994). A framework for monitoring crop growth by combining directional and spectral remote sensing information. *Remote Sensing of Environment, 50*, 161–170.

Cox, J. R., Frasier, G. W., & Renard, K. G. (1986). Biomass distribution at grassland and shrubland sites. *Rangelands, 8* (2), 67–68.

Delécolle, R., Maas, S. J., Gueril, M., & Baret, F. (1992). Remote sensing and crop production models: present trends. *ISPRS Journal of Photogrammetry and Remote Sensing, 47*, 145–161.

Detling, J. K., Parton, W. J., & Hunt, H. W. (1979). A simulation model of *Bouteloua gracilis* biomass dynamics on the North American shortgrass prairie. *Oecologia, 38*, 167–191.

Dodd, M. B., & Lauenroth, W. K. (1997). The influence of soil texture on the soil water dynamics and vegetation structure of a shortgrass steppe ecosystem. *Plant Ecology, 133*, 13–28.

Ehleringer, J., & Pearcy, R. W. (1983). Variation in quantum yield for CO_2 uptake among C_3 and C_4 plants. *Plant Physiology, 73*, 555–559.

Epstein, H. E., Burke, I. C., & Lauenroth, W. K. (1999). Response of the shortgrass steppe to changes in rainfall seasonality. *Ecosystems, 2*, 139–150.

Epstein, H. E., Lauenroth, W. K., Burke, I. C., & Coffin, D. P. (1998). Regional productivities of plant species in the great plains of the United States. *Plant Ecology, 134*, 173–195.

Fisher, A., Kergoat, L., & Dedieu, G. (1997). Coupling satellite data with vegetation functional models: review of different approaches and perspectives suggested by the assimilation strategy. *Remote Sensing Reviews, 15*, 283–303.

Franks, S. W., & Beven, K. J. (1999). Conditioning a multiple-patch model using uncertain time–space estimates of latent heat fluxes inferred from remotely sensed data. *Water Resources Research, 35* (9), 2751–2761.

Goetz, S. J., & Prince, S. D. (1998). Variability in carbon exchange and light utilization among boreal forest stands: implications for remote sensing of net primary production. *Canadian Journal of Forest Research, 28*, 375–389.

Goetz, S. J., & Prince, S. D. (1999). Modelling terrestial carbon exchange

and storage: evidence and implications of functional convergence in light-use efficiency. In: A. H. Fitter, & D. Raffaelli (Eds.), *Advances in ecological research* (vol. 28, pp. 57–92). New York: Academic Press.

Goff, B. F. (1985). Dynamics of canopy structure and soil surface cover in a semiarid grassland. Unpublished master's thesis, University of Arizona, Tucson.

Goward, S. N., & Huemmrich, K. F. (1992). Vegetation canopy PAR absorptance and the normalized difference vegetation index: an assessment using the SAIL model. *Remote Sensing of Environment, 39*, 119–140.

Gower, S. T., Kucharik, C. J., & Norman, J. (1999). Direct and indirect estimation of leaf area index, fAPAR, and net primary production of terrestrial ecosystems. *Remote Sensing of Environment, 70*, 29–51.

Hanan, N. P., Prince, S. D., & Bégué, A. (1995). Estimation of absorbed photosynthetically active radiation and vegetation net production efficiency using satellite data. *Agricultural and Forest Meteorology, 76*, 259–276.

Hanan, N. P., Prince, S. D., & Bégué, A. (1997). Modelling vegetation primary production during HAPEX-Sahel using production efficiency and canopy conductance model formulations. *Journal of Hydrology, 188–189*, 651–675.

Hanson, J. D., Skiles, J. W., & Parton, W. J. (1988). A multispecies model for rangeland plant communities. *Ecological Modelling, 44*, 89–123.

Hazlett, D. L. (1992). Leaf area development of four plant communities in the Colorado steppe. *American Midland Naturalist, 127* (2), 276–289.

Hook, P. B., Lauenroth, W. K., & Burkes, I. C. (1994). Spatial patterns of roots in a semiarid grassland: abundance of canopy openings and regeneration gaps. *Journal of Ecology, 82*, 485–494.

Inoue, Y., Moran, M. S., & Horie, T. (1997). Predicting potential and actual crop growth and yield based on a simulation model with remotely sensed spectral measurements. In: Proc. of 7th International symposium in remote sensing, Courchevel, France, 7–11 April 1997.

Jacquemoud, S., & Baret, F. (1990). PROSPECT: a model of leaf optical properties spectra. *Remote Sensing of Environment, 34*, 75–91.

Jacquemoud, S., Baret, F., & Hanocq, J. F. (1992). Modeling spectral and bidirectional soil reflectance. *Remote Sensing of Environment, 41*, 123–132.

Jacquemoud, S., Ustin, S. L., Verdebout, J., Schmuck, G., Andreoli, G., & Hosgood, B. (1996). Estimating leaf biochemistry using the PROSPECT leaf optical properties model. *Remote Sensing of Environment, 56*, 194–202.

Jackson, R. B., Canadell, J., Ehleringer, J. R., Mooney, H. A., Sala, O. E., & Schulze, E. D. (1996). A global analysis of root distributions for terrestrial biomes. *Oecologia, 108*, 389–411.

Jackson, R. D., Teillet, P. M., Slater, P. N., Fedosejevs, G., Jasinski, M. F., Aese, J. K., & Moran, M. S. (1990). Bidirectional measurements of surface reflectance for view angle corrections of oblique imagery. *Remote Sensing of Environment, 32*, 189–202.

Knight, D. H. (1973). Leaf area dynamics of shortgrass prairie in Colorado. *Ecology, 54*, 891–896.

Kucharick, C. J., Norman, J. M., & Gower, S. T. (1999). Characterization of radiation regimes in nonrandom forest canopies: theory, measurements, and a simplified modeling approach. *Tree Physiology, 19*, 695–706.

Kustas, W. P., Blanford, J. A., Stannard, D. I., Daughtry, C. S. T., Nichols, W. D., & Weltz, M. A. (1994). Local energy fluxes estimates for unstable conditions using variance data in semiarid rangelands. *Water Resources Research, 30* (5), 1351–1361.

Kustas, W. P., & Goodrich, D. C. (1994). Preface to the special issue on Monsoon 90. *Water Resources Research, 30* (5), 1211–1225.

Kuusk, A. (1995a). A Markov chain model of canopy reflectance. *Agricultural and Forest Meteorology, 76*, 221–236.

Kuusk, A. (1995b). A fast, invertible canopy reflectance model. *Remote Sensing of Environment, 51*, 342–350.

Lauenroth, W. K., & Sala, O. E. (1992). Long-term forage production of north American shortgrass steppe. *Ecological Application, 2* (4), 397–403.

Liang, Y. M., Hazlett, D. L., & Lauenroth, W. K. (1989). Biomass dynamics and water use efficiencies of five plant communities in the shortgrass steppe. *Oecologia, 80*, 148–153.

Lhomme, J. P. (1998). Formulation of root water uptake in a multilayer soil–plant model: does van den Honert's equation hold? *Hydrology and Earth System Sciences, 2* (1), 31–40.

Lo Seen, D., Chehbouni, A. G., Njoku, E., Saatchi, S., Mougin, E., & Monteny, B. (1997). An approach to couple vegetation functioning and soil–vegetation–atmosphere-transfer models for semiarid grasslands during the HAPEX-Sahel experiment. *Agricultural and Forest Meteorology, 83*, 49–74.

Luquet, D., Bégué, A., Dauzat, J., Nouvellon, Y., & Rey, H. (2001). 3D computer vegetation model, a powerful tool for radiative transfer studies–Example of the radiation interception by a *Bouteloua gracilis* dominant short-grass ecosystem. Submitted to *Agricultural and Forest Meteorology*.

Maas, S. J. (1988a). Use of remotely sensed information in agricultural crop growth models. *Ecological Modelling, 41*, 247–268.

Maas, S. J. (1988b). Using satellite data to improve model estimates of crop yield. *Agronomy Journal, 80*, 655–662.

Milchunas, D. G., & Lauenroth, W. K. (1992). Carbon dynamics and estimates of primary production by harvest $_{14}C$ dilution, and $_{14}C$ turnover. *Ecology, 73* (2), 593–607.

Monteith, J. L. (1965). Evaporation and the environment. *Symposia of the Society for Experimental Biology, 19*, 205–234.

Moran, M. S., Bryant, R., Thome, K., Ni, W., Nouvellon, Y., Gonzalez-Dugo, M. P., Qi, J., & Clarke, T. R. (2001). A refined empirical line approach for reflectance factor retrieval from Landsat-5 TM and Landsat-7 ETM+. *Remote Sensing of Environment* (this issue).

Moran, M. S., Clarke, T. R., Kustas, W. P., Weltz, M., Amer, S. A., & Huete, A. R. (1994). Evaluation of hydrologic parameters in semiarid rangeland using remotely sensed spectral data. *Water Resources Research, 30*, 1287–1297.

Moran, M. S., Maas, S. J., & Pinter, P. J. (1995). Combining remote sensing and modeling for estimating surface evaporation and biomass production. *Remote Sensing Reviews, 12*, 335–353.

Moran, M. S., Nouvellon, Y., Bryant, R. B., & Ni, W. (2000). Assimilating Landsat imagery in a grassland growth model: a case study in Arizona. In: Proc. of Pecora 14/Land Satellite Information in the Next Decade III conference, December 6–10, 1999 Denver, CO.

Moran, M. S., Rahman, A. F., Washburne, J. C., Goodrich, D. C., Weltz, M. A., & Kustas, W. P. (1996). Combining the Penman–Monteith equation with measurements of surface temperature and reflectance to map regional evaporation rates. *Agricultural and Forest Meteorology, 80*, 87–109.

Moran, M. S., Vidal, A., Troufleau, D., Inoue, Y., Qi, J., Clarke, T. R., Pinter, P. J., Mitchell, T., & Neale, C. M. U. (1997). Combining multifrequency microwave and optical data for farm management. *Remote Sensing of Environment, 61*, 96–109.

Mougin, E., Lo Seen, D., Rambal, S., Gaston, A., & Hiernaux, P. (1995). A regional Sahelian grassland model to be coupled with multispectral satellite data: 1. Model description and validation. *Remote Sensing of Environment, 52*, 181–193.

Moulin, S., Bondeau, A., & Delécolle, R. (1998). Combining agricultural crop models and satellite observations: from field to regional scales. *International Journal of Remote Sensing, 19* (6), 1021–1036.

Nelder, J. A., & Mead, R. (1965). A simplex method for function minimization. *Computer Journal, 7*, 308–313.

Nichols, M. H., Lane, L. J., Asce, M., & Manetsch, C. (1993). Analysis of spatial and temporal precipitation data over a densely gauged experimental watershed. In: Proc. of the Management of irrigation and drainage systems conference, Park City, UT, July 21–23 1993. (pp. 440–447).

Nilson, T. (1971). A theoretical analysis of the frequency of gaps in plant stands. *Agricultural Meteorology, 8*, 25–38.

Nilson, T., & Kuusk, A. (1989). A reflectance model for the homogeneous plant canopy and its inversion. *Remote Sensing of Environment, 27*, 157–167.

Nouvellon, Y. (1999). Modélisation du fonctionnement de prairies semi-

arides et assimilation de données radiométriques dans le modèle. PhD thesis, Institut National Agronomique Paris-Grignon.

Nouvellon, Y., Bégué, A., Moran, M. S., Lo Seen, D., Rambal, S., Luquet D., Chehbouni, A. G., & Inoue, Y. (2000). PAR extinction in shortgrass-ecosystems: effects of clumping, sky conditions and soil albedo. *Agricultural and Forest Meteorology, 105*, 21–41.

Nouvellon, Y., Lo Seen, D., Rambal, S., Bégué, A., Moran, M. S., Kerr, Y., & Qi, J. (2000). Time course of radiation use efficiency in a shortgrass ecosystem: consequences for remotely sensed estimation of primary production. *Remote Sensing of Environment, 71*, 43–55.

Nouvellon, Y., Moran, M. S., Chehbouni, A. G., Lo Seen, D., Bryant, R., Nichols, M., Prévot, L., Rambal, S., Ni, W., Bégué, A., Heilman, P., & Keefer, T. O. (2000). Assimilating Landsat data in an ecosystem model for multiyear simulation of grassland carbon, water and energy budgets. In: Proc. of the IEEE 2000 International Geoscience and Remote Sensing Symposium, Honolulu, HI, 24–28 July 2000.

Nouvellon, Y., Rambal, S., Lo Seen, D., Moran, M. S., Lhomme, J. P., Bégué, A., Chehbouni, A. G., & Kerr, Y. (2000). Modelling of daily fluxes of water and carbon from shortgrass steppes. *Agricultural and Forest Meteorology, 100*, 137–153.

Olioso, A., Taconet, O., & Ben Mehrez, M. (1996). Estimation of heat and mass fluxes from IR brightness temperature. *IEEE Transactions on Geoscience and Remote Sensing, 34* (5), 1184–1190.

Osborn, H. B., Lane, L. J., & Hundley, J. F. (1972). Optimum gauging of thunderstorm rainfall in southeastern Arizona. *Water Resources Research, 8* (1), 259–265.

Parton, W. J., Singh, J. S., & Coleman, D. C. (1978). A model of production and turnover of roots in shortgrass prairie. *Journal of Applied Ecology, 47*, 515–542.

Paruelo, J. M., Epstein, H. E., Lauenroth, W. K., & Burke, I. C. (1997). ANPP estimates from NDVI for the central grassland region of the United States. *Ecology, 78* (3), 953–958.

Price, J. C. (1990). On the information content of soil reflectance spectra. *Remote Sensing of Environment, 33*, 113–121.

Prince, S. D. (1991). A model for regional primary production for use with coarse resolution satellite data. *International Journal of Remote Sensing, 12* (6), 1313–1330.

Prince, S. D., & Goward, S. N. (1995). Global primary production: a remote sensing approach. *Journal of Biogeography, 22*, 815–835.

Rahman, H., & Dedieu, G. (1994). SMAC: a simplified method for atmospheric correction of satellite measurements in the solar spectrum. *International Journal of Remote Sensing, 15* (1), 123–143.

Rambal, S., & Cornet, A. (1982). Simulation de l'utilisation de l'eau et de la production végétale d'une phytocénose Sahélienne du Sénégal. *Acta Oecologica, Oecologia Plantarum, 3* (17/4), 381–397.

Rambal, S., Lacaze, B., Mazurek, H., & Debussche, G. (1985). Comparison of hydrologically simulated and remotely sensed actual evapotranspiration from some Mediterranean vegetation formations. *International Journal of Remote Sensing, 6*, 1465–1482.

Rambal, S., Romane, F., & Aguilar-Martin, J. (1977). Modélisation de la production de biomasse végétale de la steppe sud tunisienne par une méthode globale d'estimation des paramètres et par filtrage non linéaire. Modélisation et maîtrise des systèmes techniques, économiques et sociaux, Ed. Hommes et Techniques, pp. 536–548.

Renard, K. G., Lane, L. J., Simanton, J. R., Emmerich, W. E., Stone, J. J., Weltz, M. A., Goodrich, D. C., & Yakowitz, D. S. (1993). Agricultural impacts in an arid environment: Walnut Gulch studies. *Hydrological Science and Technology, 9* (1–4), 145–190.

Ruimy, A., Saugier, B., & Dedieu, G. (1994). Methodology for the estimation of terrestrial net primary production from remotely sensed data. *Journal of Geophysical Research, 99*, 5263–5283.

Running, S. W., Baldocchi, D. D., Turner, D. P., Gower, S. T., Bakwin, P. S., & Hibbard, K. A. (1999). A global terrestrial monitoring network integrating tower fluxes, flask sampling, ecosystem modeling and EOS satellite data. *Remote Sensing of Environment, 70*, 108–127.

Running, S. W., Nemani, R. R., Peterson, D. L., Band, L. E., Potts, D. F., Pierce, L. L., & Spanner, M. A. (1989). Mapping regional forest evapotranspiration and photosynthesis by coupling satellite data with ecosystem simulation. *Ecology, 70* (4), 1090–1101.

Ryle, G. J. A. (1970). Partition of assimilates in an annual and a perennial grass. *Journal of Applied Ecology, 7*, 217–227.

Saugier, B. (1992). Production primaire: Du chloroplaste à la biosphère. Hiérarchies et échelles en écologie. Ed. Naturalia, pp. 65–84.

Saxton, K. E., Rawls, W. J., Romberger, J. S., & Papendick, R. I. (1986). Estimating generalized soil–water characteristics from texture. *Soil Science Society of America Journal, 50*, 1031–1036.

Sellers, W. D., & Hill, R. H. (1974). Arizona climate 1931–1972. The University of Arizona Press, Tucson.

Sims, P. L., & Singh, J. S. (1978). The structure and the function of ten western north American grasslands: II. Intraseasomal dynamics in primary producer compartments. *Journal of Ecology, 66*, 547–572.

Sims, P. L., Singh, J. S., & Lauenroth, W. K. (1978). The structure and the function of ten western north American grasslands: I. Abiotic and vegetational characteristics. *Journal of Ecology, 66*, 251–285.

Singh, J. S., & Coleman, D. C. (1975). Evaluation of functional root biomass and translocation of photoassimilated carbon-14 in a shortgrass prairie ecosystem. In: J. K. Marshall (Ed.), *The belowground ecosystem: a synthesis of plant associated processes* (pp. 123–131). Stroudsburg, PA: Dowden Hutchison and Ross.

Smith, R. E., Goodrich, D. C., Woolhiser, D. A., & Unkrich, C. L. (1995). KINEROS — a kinematic runoff and erosion model. In: V. J. Singh (Ed.), *Computer models of watershed hydrology* (pp. 697–732). Highlands Ranch, CO: Water Resources Pub.

Stannard, D. I., Blanford, J. H., Kustas, W. P., Nichols, W. D., Amer, S. A., Schmugge, T. J., & Weltz, M. A. (1994). Interpretation of surface flux measurements in heterogeneous terrain during the Monsoon '90 experiment. *Water Resources Research, 30* (5), 1227–1239.

Taconet, O., Olioso, A., Ben Mehrez, M., & Brisson, N. (1995). Seasonal estimation of evaporation and stomatal conductance over a soybean field using surface infrared temperature. *Agricultural and Forest Meteorology, 73*, 321–337.

Tanré, D., Deroo, C., Duchaud, P., Herman, M., Morcrette, J. J., Perbos, J., & Deschamps, P. Y. (1990). Description of a computer code to simulate the satellite signal in the solar spectrum: the 5S code. *International Journal of Remote Sensing, 11*, 659–668.

Tiscareno-Lopez, M. (1994). A Bayesian-Monte Carlo approach to access uncertainties in process-based, continuous simulation models. PhD thesis, University of Arizona, Tucson.

Toth, J. J. (1997). Coupling Landsat data with a mesoscale model to estimate evapotranspiration. In: Proc. of the AMS 13th Conf. on Hydrology, 2–7 February, Long Beach, CA. p. 9.6.

Tueller, P. T. (1989). Remote sensing technology for rangeland management applications. *Journal of Range Management, 42*, 442–453.

Verhoef, W. (1984). Light scattering by leaf layers with application to canopy reflectance modeling: the SAIL model. *Remote Sensing of Environment, 16*, 125–141.

Webb, W., Szarek, S., Lauenroth, W., Kinerson, R., & Smith, M. (1978). Primary productivity and water use in native forest, grassland, and desert ecosystems. *Ecology, 59* (6), 1239–1247.

Weltz, M. A., Ritchie, J. C., & Fox, H. D. (1994). Comparison of laser and field measurements of vegetation height and canopy cover. *Water Resources Research, 30* (5), 1311–1319.